PLASTICITY ENHANCEMENT OF BULK METALLIC GLASSES BY METAL ELECTROPLATING

CHEN Wen

M.Phil

The Hong Kong

Polytechnic University

2012

The Hong Kong Polytechnic University

Department of Industrial and Systems Engineering

PLASTICITY ENHANCEMENT OF BULK METALLIC GLASSES BY METAL ELECTROPLATING

by

CHEN Wen

A Thesis Submitted in Partial Fulfillment of the

Requirements for the Degree of Master of Philosophy

August 2011

CERTIFICATE OF ORIGINALITY

I hereby declare that this dissertation is my own work and that, to the best of my knowledge and belief, it reproduces no material previously published or written nor material which has been accepted for the award of any other degree or diploma, except where due acknowledgements has been made in the text.

_____ (Signed)

CHEN Wen (Name of Student)

Abstract

Bulk metallic glasses (BMGs), first synthesized during the 1970s, have stimulated great research interest because of their unique properties. In the past decades, although significant progress has been achieved in understanding the atomic structure and properties of these materials, poor room temperature deformability still hinders their wide commercial applications. In contrast to crystalline materials that deform through dislocation movements, the plastic deformation of BMGs at room temperature is highly localized in shear bands that proceed and cross over the specimen rapidly, resulting in limited plasticity.

Many approaches have been so far developed for plasticity enhancement of BMGs, such as the in situ formation of crystalline phases, the achievement of a critical value of Poisson's ratio, and the imposition of geometric confinement. Among these approaches, metal electroplating has been proven to be feasible in toughening Zr-based BMGs. However, its effect on other types of BMGs, and a detailed analysis on the underlying mechanism for the plasticity enhancement by coating confinement have yet to be undertaken. In the present work, the effect of Ni coating on $Zr_{57}Al_{10}Ni_8Cu_{20}Ti_5$ and $Fe_{75}Mo_5(P_{50}C_{41.67}B_{8.33})_{20}$ BMGs were further analyzed. Both of the BMGs have exhibited higher plastic strains than their uncoated counterparts, manifesting that the Ni coating is an effective way in toughening these types of BMG. The increased plasticity is believed to be

attributed to the nucleation of profuse shear bands and the impedance of shear band propagation due to the imposed confining effect of the Ni coating.

In the present work, a Cu/Ni bilayered coating was also electrodeposited onto a $Zr_{57}Al_{10}Ni_8Cu_{20}Ti_5$ BMG. It demonstrated for the first time that the effectiveness of geometric confinement in toughening BMGs by the bilayered coating outweighed that by a mono-layered Cu or Ni coating with equivalent thickness. The inner soft Cu layer in the Cu/Ni coating behaves as a good "crack buffer zone" to effectively absorb the elastic deformation energy released by BMGs; while the outer strong Ni layer and the strong Cu/Ni interface assisted in strengthening the geometric confinement.

By combining the effect of geometric confinement and the reduction of friction at the boundaries, remarkable plasticity enhancement was also reported for the first time in the Cu-coating encapsulated $Zr_{57}Al_{10}Ni_8Cu_{20}Ti_5$ BMG. With the aid of the Cu coating as a lubricant, the elastic mismatch between the loading platens and the specimen was reduced, and the Cu coatings at two ends could generate a lateral pressure near the edges of the specimen. Accordingly, the lateral spreading of the material near the ends was promoted and the plasticity of the BMG was improved. Besides, a non-homogeneous microstructure was observed in the Cu coated BMGs during the deformation, which was also considered to contribute to the enhanced plasticity of BMGs. The findings of the current work not only lead

to a better understanding of the geometric confinement effect, but also lay down a good foundation for further optimizing this technique for plasticity enhancement of BMGs.

Acknowledgements

First and foremost, I would like to express my deep gratitude to my supervisor, Prof. K.C. Chan for giving me this great opportunity to join his group and learn from him every day. I am indebted to him for offering the inspiring ideas for my research and bringing me to the fantastic world of bulk metallic glasses. He has, certainly, instructed me about scientific inquiries, but the lessons I learned from him include responsibility, integrity and also professionalism, which will remain along with me always in my future life. I would like to deeply appreciate for his unwavering trust that makes me believe anything is possible for me, and for his insightful inspiration on science that aids me to ever advance. Without his continuous encouragements and guidances over the past two years, I would not have completed this thesis.

I am truly benefited from all the resources in the group. Many thanks go to Dr. Peng Yu, Mr. Ze Liu, and Mr. Shunhua Chen in our research group for their warm help with my specimen preparations and mechanical tests. I would like to express my particular gratitude to Mr. S.Y. Lau, the technician in our lab, for his patience and thoroughness in instructing me to use those equipments for my experiments.

Special thanks go to Dr. Gang Wang (Shanghai University, China), Dr.

Shengfeng Guo (Huazhong University of Science and Technology, China), and Dr. Weihuo Li (Anhui Institute of Technology, China) for their experimental assistances as well as stimulating discussions on my works.

If there were anybody deserving special awards, it would have to be my lovely parents, who do everything they could to support my sister and me. Thanks to them for hanging in there, believing me and supporting me all the time. I am also grateful to my sister for her dedication to taking care of our parents.

The research work presented in this thesis was financially supported by the Research Committee of The Hong Kong Polytechnic University. I would like to sincerely acknowledge this substantial support for my work.

Table of Contents

List of Figures

List of Tables

Chapter 1 Introduction

1.1 Background

Traditional metallic materials are crystalline solids in nature, and their mechanical properties are governed by their dislocation systems and grain structures. Whereas, bulk metallic glasses (BMGs, or bulk amorphous alloys) have a unique microstructure of random atomic configurations in the absence of the lattice order, dislocation networks and grain structures. Since this class of metallic material is a non-crystalline solid in nature, there are no lattice defects such as dislocations and grain boundaries. Due to their unique structures, BMGs possess many unique properties that are different from crystals, including ultrahigh theoretical strength, excellent corrosion resistance, high elastic strain limit, good fatigue resistance as well as good workability in the supercooled liquid region [1-5]. This has aroused cumulative interest in exploiting the commercialization potential for BMGs, in such fields as golf club heads and microelectromechanical systems (MEMS) [6, 7]. Overall, plasticity is an important mechanical index to assess the success of any material for structural applications. Disappointingly, BMGs generally exhibit negligible plastic deformability at ambient temperature due to the lack of dislocation networks as in crystalline solids. Upon yielding, the plastic deformation of BMGs at room temperature is achieved through shear localization, and the shear plastic strain is highly localized into nano-scaled shear bands. These narrow shear bands

propagate rapidly across the sample after their initiation, leading to limited ductility before macroscopic catastrophic failure behavior, which has become one major shortcoming restricting the wide application of BMGs as structural engineering materials [8-11].

In fact, plasticity is a very ambiguous term. If plasticity is defined in terms of the plastic strain from yield to failure, irrespective of where the plastic strain is distributed, then BMGs are extraordinary ductile as most of the deformation is concentrated in the narrow shear bands, where the plasticity could even exceeds 100%. Unfortunately, BMGs can hardly show significant macroscopic plasticity. Therefore, BMGs that exhibit a super-high plasticity in the shear bands cannot properly be termed as macroscopically ductile materials. Since the ductility of BMGs is controlled by shear band operations, the philosophy of enhancing the plasticity of BMGs is to postpone the rapid propagation of shear bands, stabilize the shear banding behavior and thus activate multiple shear bands. Generally, the more the shear bands, the higher the plasticity. In past years, with all the efforts in studying the atomic structure and mechanical behavior of BMGs, the plastic deformation behavior of BMGs has being increasingly understood, leading to the development of many new toughening methods. The prevailing methods to toughen BMGs can be essentially grouped into two categories: 1) intrinsic microstructure manipulation; 2) extrinsic modification. The former one can be achieved by compositional modification or incorporation of a secondary

crystalline phase to hamper the shear band propagation and form multiple shear bands [3]. The latter method can be reached by controlling extrinsic conditions, from which the plastic deformation of BMGs can benefit. For instance, the introduction of residual stress on the surface of BMGs [12] and the optimization of frictional boundary restraints by using a Cu foil lubricant [13] can contribute to an improved plasticity.

Although numerous works have been conducted to study the factors influencing the mechanical properties of BMGs, due to the complexity of the real deformation mechanism of BMGs, more efforts are needed to develop futher engineering techniques or strategies to toughen BMGs.

1.2 Motivations and objectives

It is well known that the mechanical behavior of a large number of brittle materials, like conventional silicate glasses, is very sensitive to the surface state, which may directly influence the ultimate plastic deformation and fracture behavior [14]. Since most failures of BMGs initiate from the surface, the fracture morphologies and shear band distribution at the surface of deformed BMGs have been analyzed in order to understand their plastic deformation. It is expected that the plasticity enhancement of BMGs can be embarked on from the perspective of surface modification. In fact, improving the plasticity of BMGs via manipulation of shear banding behavior in the surface or subsurface through residual stress

control [12], shrink-fit metal sleeve confinement [15], metal coating confinement [16] and reduction of contact friction at the compressive loading boundaries [13] has been the focus of some previous studies. Of these surface modification techniques, Cu and Ni coating electroplating have both been proven to be feasible in toughening Zr-based BMGs [16, 17]. They attribute the enhanced plasticity to the geometric confinement induced activation of multiple shear bands (or increase in shear band density). However, a detailed analysis on how the geometric confinement affects the plastic flow behavior has yet to be done.

Among the various existing BMG systems, Fe-based BMGs are well known as possessing great commercial potential and have attracted tremendous research interest due to their good magnetic properties, ultrahigh strength as well as low material cost [18-23], but the critical problem of the ultrahigh strength Fe-based BMGs is that they are far more brittle than most other BMG systems. Besides, Fe-based BMGs normally show the distinct fracture behaviour of explosive fragmentation compared with other more ductile BMGs (e.g. Zr-based or Cu-based BMGs) [24, 25]. It is therefore of significance to further investigate the effect of metal coatings on the plasticity of ultrahigh strength Fe-based BMGs, and to understand the flow behavior of different BMG systems.

In studying the geometric confinement of BMGs, some researchers have found that a ductile layer (of the order of ~20 μm) of Cu coating closely adjacent to

BMGs can act as a good "crack buffer zone" to absorb the strain and the elastic energy release caused by the deformation induced surface steps, thereby effectively suppressing the crack formation and delaying the final fracture of BMGs [17]. From this standpoint, the coating layer electroplated onto BMGs should be sufficiently ductile to translate the shear band propagation energy into its own plastic deformation. Typically, Cu electrodeposits obtained from an acid sulphate solution exhibit considerable ductility (11% ~ 16% tensile elongation) with a relatively low yield strength of 120 ~ 150 MPa [26], suitable to behave as a "crack buffer zone". On the other hand, for guaranteeing effective lateral geometric confinement, the yield strength of the outer confining metal layer should be high enough, which has been proven in studying the lateral confinement of glass ceramic materials [27, 28]. Ni electroplating from the Hard Watts electrolyte (containing ammonia ions) at room temperature is able to produce a strong layer of Ni coating with tensile strength as high as around 1000 MPa but with limited ductility [29]. Therefore, it is of great interest to synthesize a bilayered Cu/Ni coating exhibiting both the above two mechanisms for the enhancement of the plasticity of BMGs.

Furthermore, by inserting Cu foils at the interfaces between the loading platens and the two ends of the BMGs to reduce the friction at the loading boundaries, an enhancement of plasticity of BMGs was reported [13]. It is of great significance to further toughen BMGs by encapsulating a BMG with a Cu coating, so that the

Cu coatings on the two ends of the BMGs would act as a solid lubricant, and the lateral Cu coating on the side surface can apply a lateral geometrical confinement to the BMGs. It is expected that the encapsulated BMGs with a combined effect of geometric confinement and friction reduction can achieve more pronounced plastic strain before catastrophic failure.

In the present work, the prime aim is therefore to enhance the plasticity of BMGs by tailoring extrinsic measures, including geometric confinement and optimization of testing conditions through the technique of metal electroplating. The specific objectives of the project are:

1. To enhance the plasticity of both Zr-based and Fe-based BMGs by lateral metal coating confinement.
2. To compare and understand the geometric confinement effect on plasticity enhancement of BMGs using mono-layered Cu, mono-layered Ni coating, and bilayered Cu/Ni coatings.
3. To investigate the influence of frictional boundary conditions on the uniaxial compressive behaviour of BMGs.
4. To understand the combined effect of geometric confinement and friction reduction at loading boundaries on plasticity of BMGs.

1.3 Outline of thesis

In Chapter 1, the background information and the detailed research objectives of this present work are presented. In Chapter 2, the historical development of BMGs, the glass forming ability of BMGs, the homogeneous and inhomogeneous plastic flow behavior of BMGs are briefly introduced, followed by a review of the recent development of plasticity improvement of BMGs. The detailed experimental procedures in this work are described in Chapter 3, where the detailed electroplating processes, compression testing and characterization techniques are introduced. In Chapter 4, the X-ray diffraction (XRD) results are presented and the thermal behavior of the BMG specimens are reported. In Chapter 5, the geometric confinement effect by a lateral Ni electroplated coating as well as a Cu/Ni bilayered coating on the plasticity enhancement is discussed. In Chapter 6, the mechanical behavior of a Cu-coating encapsulated BMG is compared with that of the uncoated, laterally Cu-coated, and two ends Cu-coated specimens. In Chapters 5 and 6, the disparities in shear banding behavior of different samples and some phenomena during mechanical testing are also discussed primarily based on close analysis of compressive stress-strain curves as well as fracture morphologies. Moreover, to understand the mechanical behavior of BMGs with and without electroplated coatings, the underlying reasons and mechanisms accounting for the differences in compression results are formulated. Chapter 7 gives the conclusions of the work, and some future work is suggested in Chapter 8.

Chapter 2 Literature review

2.1 Historical development of bulk metallic glasses (BMGs)

Conventional crystalline materials possess translational symmetry, i.e., the constitutional atoms are arranged in long periodic orders. In contrast, metallic glasses or non-crystalline alloys are a class of metal alloys where atoms are almost randomly arranged with only short-to-medium range orders. Generally, metallic glasses are obtained by means of the rapid solidification technique of the liquid alloys from the melts. This concept of metallic materials was firstly brought about in the 1960s when Duwez's group in Caltech successfully synthesized an Au-Si metallic glass alloy by quenching at the order of 10^6 K/s [30]. In fact, when a liquid is undercooled, crystallization typically happens and the liquid transforms into a crystalline solid. However, with the development of the rapid solidification technique, many traditional concepts of metallurgical science have been revolutionized. Since the cooling rate in the rapid solidification technique is so fast that the constitutional atoms are deprived of the opportunity to nucleate and crystallize to their normal crystalline state, but rather tend to be hastily frozen, in which case metallic glasses or quasicrystalline materials (where traditional forbidden rotational symmetries are found) can be attained. The most significant difference between the metallic glass forming alloys and the normal metallic alloys is that the former alloy liquid is able to be substantially undercooled without crystallization, either because of the exertion

of a very high cooling rate, or due to the absence of heterogeneous nucleation sites, the initial high viscosity of the liquid, the large interfacial energy between the melt and the crystal, or some other reasons.

It is notable to point out that in the process of continuous cooling solidification, the viscosity of the metallic glass liquid increases with the decrease of temperature. Normally, the temperature at which the viscosity of the liquid reaches a certain value of 10^{12} Pa·s is defined as the glass transition temperature T_g, below which the viscosity is high enough and the liquid is "frozen-in" to form a metallic glass. Hence, metallic glasses, in nature, are a family of non-equilibrium phase of matter for which the equilibrium solidification process is suppressed by a kinetic barrier [31]. Upon reheating, a metallic glass solid can be rapidly heated back to the supercooled liquid region without crystallization, and this glass-liquid transition is deemed as reversible in the supercooled liquid region. However, if the heating temperature exceeds a high value of T_x, i.e., the onset crystallization temperature or the endpoint temperature of the supercooled liquid interval ΔT_x ($=T_x - T_g$), the transformation from the undercooled liquid into crystalline phases usually takes place by means of atomic rearrangement due to the driving force of the crystallization induced free energy reduction.

At the early stage of metallic glasses preparation by the rapid solidification process, in order to achieve an extremely high cooling rate (10^6 K/s) to rapidly

extract the heat from the melt, it was widely recognized that at least one of the spatial dimensions of the specimen should be diminished and be quite small, like ribbons, powders or microwires of the order of only 20 ~ 50 μm. This, beyond doubt, had been limiting the applications of metallic glasses. Therefore, following the first success in the preparation of Au-Si metallic glass by the Duwez group, a lot of effort was spent in improving the ability of producing metallic glasses with a slower quenching speed, in which case specimens of thicker dimensions can be produced. Fortunately, a considerable number of breakthroughs were achieved in the synthesis of "bulk" metallic glasses at relatively slower quenching speeds in the 1980s, when several research groups found that the crystallization process could be suppressed in those alloys with compositions at deep eutectics whose constituents have a wide range of atomic sizes [32-37]. Bulk metallic glass (BMG) rods with millimeter diameters were firstly discovered by Chen *et al* in the Pd-Cu-Si ternary system at a cooling rate of 10^3 K/s [38], which opened a new spectrum for BMGs to be used as structural engineering components. Later, BMGs of large sizes continued to attract strong attention among many scientists. Numerous prominent works have been reported over the past decades. In 1984, Greer and Turnbull *et al* [36] produced centimeter-sized Pd-Ni-P BMGs at a slow cooling rate of only 10 K/s by the fluxing method. In 1989, the Inoue group [39] at Tohoku University, Japan reported a 1.2 mm diameter BMG rod in the composition of $La_{55}Al_{25}Ni_{20}$ via water quenching, which was the first metallic glass alloy reported without noble

metal elements. This work stimulated increasing interest in the synthesis of more BMG alloy systems in the past decades. A wide variety of BMGs, including Mg-, Zr-, Ti-, Fe-, Co-, Ni-, Nd-, Cu-, Pr-, Ce-, Pt-based systems were subsequently developed at slow cooling rates by many research groups [1, 40-48]. Of these accomplishments, the discovery of the $Zr_{41.2}Ti_{13.8}Cu_{12.5}Ni_{10}Be_{22.5}$ (Vit1 alloy) BMG made by Peker and Johnson at Caltech was a breakthrough [41]. The temperature-time-transition (TTT) diagram of this alloy has a distant "nose" for crystal nucleation at a large time scale of 10^2 s, representing a quite low critical cooling rate of only 1 K/s for glass formation in this composition. This Zr-based BMG, possessing a wide supercooled liquid region and strong thermal stability in the undercooled state, could be produced into rods ranging from 5 cm to 10 cm by the conventional casting method without any presence of crystalline phases. In addition, superior mechanical properties of this Zr-based BMG amounted to its strong industrial application potential in the three years after its birth.

In summary, it is the availability of these diverse "bulk" metallic glasses that increasingly has been stimulating more scientists to step into this area. In the past years, extensive work has been conducted on these materials, and significant progress has been achieved in understanding glass formation, preparation, atomic structure as well as properties of this category of materials.

2.2 Glass forming ability

For an alloy liquid, the ability to be significantly undercooled at temperatures below its melting temperature T_ℓ and frozen into a metallic glass without crystallization below the glass transition temperature T_g during the continuous cooling solidification process is defined as glass forming ability. In spite the fact that a great diversity of BMGs in different alloy systems have been discovered so far, for the purpose of exploring more metallic glasses in a reasonable way, it is essential to understand the underlying reasons for metallic glass formation from the melts, which can in turn aid people in designing and producing BMGs in large quantities with high reproducibility.

A couple of criteria have been developed to predict or explain the glass forming ability of BMGs that are produced by the rapid solidification method. The widely recognized criteria include critical cooling rate R_c, Inoue's criteria, reduced glass transition temperature T_{rg}, width of supercooled liquid region ΔT_x and γ parameter.

Although R_c is a criterion that can directly reflect the glass forming ability of a metal liquid, it is extremely difficult to measure this parameter in practice. The best and most convenient way to experimentally determine R_c is derived from the measured TTT diagram, as shown in Fig. 2.1 [49]. The TTT diagram stands for, at a given temperature, the time required for crystal nucleation to begin from the liquid, i.e., onset time span for isothermal crystallization as a function of

temperature. From this diagram, it is easy to appreciate that if the liquid is cooled at an exceedingly slow rate, a very long time is needed to initiate the liquid-to-crystal phase transformation. If the cooling rate is slightly faster, like described in Curve "1", solidification and crystallization starts at temperature T_1, a little below the melting temperature of the alloy T_ℓ. If the cooling rate, however, is faster than the critical cooling rate R_c, designated by Curve "2", the liquid alloy can be kept down to the undercooled state and can continue to be frozen when cooled to temperatures below T_g bypass crystallization. This critical cooling rate represented by the tangent to Curve "2" at the nose can be roughly estimated according to the following function directly:

$$\mathrm{R_c} \cong \frac{T_l - T_n}{T_n}, \tag{2.1}$$

where T_n corresponds to the nose temperature of the TTT diagram.

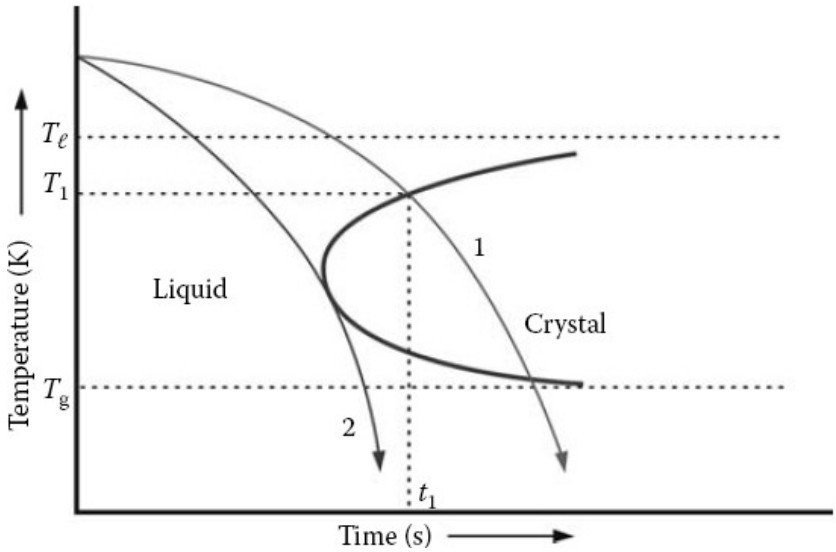

Fig. 2.1 Schematic time-temperature-transformation (TTT) diagram for a hypothetical alloy [49].

In reality, however, due to the fact that BMGs are usually formed under

continuous cooling solidification rather than in an isothermal process, the real R_c value always deviates from the estimated value derived from the above function. To address this problem, Johnson at Caltech [18] developed another function to estimate R_c as:

$$R_c = \frac{10}{d^2} \quad , \tag{2.2}$$

in which d represents the section dimension of the specimens. Apparently, the lower the R_c is, the stronger the glass forming ability will be for a hypothetical alloy.

In 2000, on the basis of thermodynamics and the kinetics of crystallization as well as the large quantity of data generated in the process of synthesis of various BMG systems, Inoue *et al* [1, 50-52] put forward three empirical rules which can be adopted to help to evaluate the glass forming ability of metallic glasses and to select bulk metallic glass systems: 1) multicomponent alloy system composed of more than at least three elements, in which the glass forming ability increases with the increase of constitutional elements; 2) different atomic size ratios among the main constituent atoms (above 12%); 3) negative heat of mix among the constituent elements. They claimed that the special atomic configurations in the alloys that conform to these three rules favor the glass forming in terms of thermodynamics and kinetics.

During continuous cooling solidification from the melting temperature T_ℓ, the

viscosity of the melt increases with the decrease of temperature. In this respect, if T_g is quite close to T_ℓ, it is expected that it is much easier for the melt to rapidly pass through this narrow temperature region and to be cooled to temperatures below T_g, where the viscosity of the melt reaches 10^{12} Pa·s and forms a metallic glass. Therefore, Turnbull [53] defined a parameter called "reduced glass transition temperature" T_{rg} to estimate the glass forming ability of the liquid alloys:

$$\mathrm{T_{rg}} = \frac{T_g}{T_\ell} . \tag{2.3}$$

That is to say, a metallic liquid with a high value of T_g and a low value of T_ℓ will favor the ability to form a metallic glass. In general, a minimum value of 0.4 for T_{rg} is necessary for an alloy to form a metallic glass, and this empirical rule has been confirmed in a number of metallic glass systems [54-58]. It is notable that many BMGs with excellent glass forming ability, like Pd-Si, Cu-Zr, Pd-P, Zr-Ti-Cu, are deep eutectics, judging from the phase diagrams. The ease of glass formation for these eutectic alloys can be primarily attributed to the higher T_{rg} with the reduction of the melting temperature T_ℓ.

Another frequently used indicator to reflect the glass forming ability of an alloy is the width of the supercooled liquid region; the ΔT_x criterion. It has been widely agreed that a larger ΔT_x value suggests a more superior thermal stability to resist the crystallization process for a metallic glass. Inoue [1, 59], based upon this, deduced a close correlation between the interval of the supercooled liquid region

and the glass forming ability. He claimed that the glass forming ability increases with the increase of ΔT_x and this criterion has been confirmed in a vast number of metallic glasses [60]. However, in some metallic glasses such as La-Al-Cu-Ni and Pd-Cu-Ni-P alloys, exceptions to this rule and the discrepancy between T_{rg} criterion and ΔT_x criterion in assessing the glass forming ability have been discovered [61, 62]. Attempting to overcome this problem, Lu and Liu [63, 64] proposed another parameter, namely the γ parameter, to gauge the glass forming ability. They combined two stability (capability of resistance to crystallization) parameters of metallic glass alloys, 1/2 (T_g + T_ℓ) and T_x, together to deduce a new parameter γ as:

$$\gamma = \frac{T_x}{T_g + T_\ell} \tag{2.4}$$

The higher γ is, the stronger is the glass forming ability. Although γ provides a better reference in assessing the glass forming ability for most metallic glasses with eutectic compositions, it shows less accuracy in evaluating the glass forming ability for metallic glasses whose composition depart from eutectics [65].

Later on, some new work developed other norms for assessing the glass formation of liquid alloys such as viscosity [66] and the new δ parameter [67]. In fact, on the basis of all these analyses, it is appreciated hitherto that not one single parameter is able to satisfactorily predict or evaluate the glass forming ability in all metallic glass alloy systems. More work, therefore, is still needed to

integrate all impacting factors of glass forming ability and postulate a more universal parameter.

2.3 Flow and plastic deformation of BMGs

Due to progress in the research of glass forming ability, many families of bulk metallic glasses have been exploited. This, in turn, provides materials scientists with many more opportunities to conduct some fundamental investigations on the structure and properties of BMGs. In order to exploit the structural applications for BMGs, it is significant to study the flow and deformation behavior of BMGs.

2.3.1 Homogeneous and inhomogeneous deformation modes

Under external loading, two distinct deformation modes of BMGs were discovered by Spaepen in 1977 [68]: homogeneous and inhomogeneous flow behavior. The former usually occurs at low stresses and high temperatures (e.g., above ~ 0.7 T_g) while the latter takes place at high stresses and low temperatures. The homogeneous deformation of BMGs can been treated as a type of spatial viscous flow, resulting in superplasticity, and is therefore significant for the exploitation of industrial applications such as net-shaping forming and superplastic forming [69-73]. Fig. 2.2 is an example of the superplastic deformability of a Cu-based BMG at a temperature in the supercooled liquid region at a strain rate of 3×10^{-3} s^{-1}.

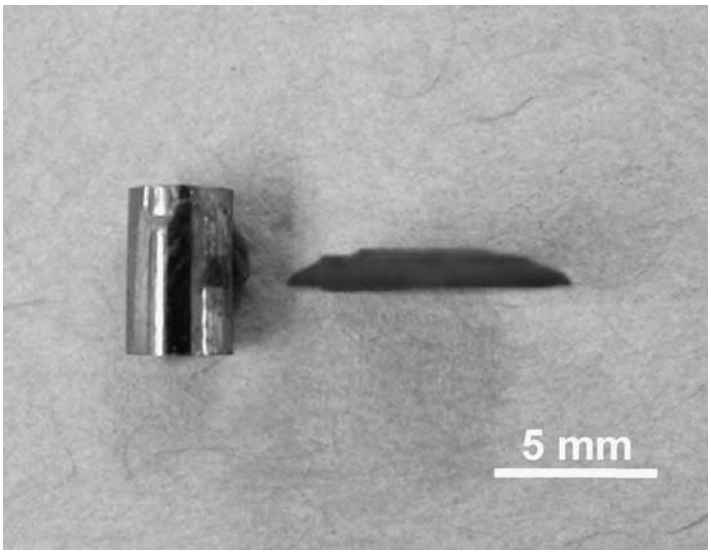

Fig. 2.2 Edge view of $Cu_{60}Zr_{20}Hf_{10}Ti_{10}$ BMG before and after testing in compression at 740 K [69].

Generally, the plastic deformation of crystalline solids is greatly dependent on defects such as dislocations, point defects and grain boundaries within the materials. The plastic deformation of crystalline materials is launched and developed by the movements of dislocations, which interact with each other or other crystalline defects and thus provide the crystalline materials with "work-hardening" ability. In sharp contrast, unlike crystalline materials, the plastic deformation of BMGs at low temperatures and high stresses is usually associated with inhomogeneous plastic flow behavior, highly localized in shear bands, which propagate seemingly unimpeded, giving rise to catastrophic fracture without any predictable symptoms [74-76]. Under tensile loading, plastic deformation of BMGs tends to be highly concentrated in just a single localized shear band, associated with shear banding and subsequent cracking instabilities behavior [2, 77]. While in most of other loading modes such as compression and

bending, plastic displacement is achieved in a shear mode via formation of shear bands in succession, which propagate rapidly and then sweep across the specimen to form "slip steps" on the side surface of the BMG, leading to elastic-perfectly plastic behavior [78]. Thus, a considerable number of monolithic BMGs exhibit nearly zero plastic strain under tensile loading and undergo limited plasticity (<2.0%) under compression at room temperature [2]. Although the inhomogeneous formation of shear bands plays a significant role in deriving the strength, plastic character and toughness of BMGs as engineering materials, the real mechanism underlying this inhomogeneous flow is still under debate and has become the common goal of many researchers.

2.3.2 Free volume model and shear bands

An as-cast metallic glass is metastable thermodynamically and always possesses a non-equilibrium content of residual free volume within it. The free volume in a glassy structure can be treated as a flow defect that is connected with opened atomic-scale spaces. The amount of the free volume can be continuously reduced by structural relaxation towards the more stable phase configuration such as in the case of low-temperature annealing induced structural relaxation [79]. Meanwhile, it should be noted that the external applied stresses can help generate more free volume. It is due to the stress induced coalescence and increase of the residual free volume that the localization of the shear deformation is usually accompanied by a work-softening mechanism arising from a dramatic localized

decrease in viscosity. Turnbull and Cohen [80] proposed a statistical distribution to describe the free volume in the metallic glasses. This statistical theory indicates that a shear load applied on the metallic glasses can transform the atomic diffusion tendency from an originally random probability to any direction to a preferential direction along the shearing direction so as to accommodate the shear deformation. Based on this assumption, Spaepen *et al* [68, 81] firstly developed a constitutive model, namely the free volume model, to describe the plastic deformation behavior of BMGs. As shown in Fig. 2.3 [68], the applied shear stress can bias the energy barrier for an atom to fulfill a jump step along the shearing direction by

$$\Delta G = \tau\Omega - \Delta G^{e}, \tag{2.5}$$

in which τ is the applied shear stress, Ω is the atomic volume while ΔG^{e} is the required elastic energy to fit an atom with volume v^{*} (a hard-sphere atomic volume) into a hole with volume v. From Fig. 2.3, envisioned by Spaepen, free volume is created by the applied shear stress while in the mean time the atomic jumps can also annihilate the free volume. The net change of the amount of free volume versus the time t can be characterized quantitatively by the following expression:

$$\frac{\partial v_f}{\partial t} = v^{*} v_0 \exp[-\frac{\Delta G^{m}}{k_B T} - \frac{\alpha v^{*}}{v_f}]\{\frac{2\alpha k_B T}{S v_f}(\cosh\frac{\tau\Omega}{2k_B T} - 1) - \frac{1}{n_D}\}, \tag{2.6}$$

where v_f is the average free volume per atom, α is a geometrical factor of order unity, v_0 represents the frequency of atomic vibration, ΔG^{m} is the activation energy, k_B is Boltzmann's constant, T is the absolute temperature, Ω is the atomic

volume, n_D is the number of atomic jumps required to annihilate an amount of free volume equal to v^*, while S can be calculated according to:

$$S=\frac{2}{3}\frac{1+\upsilon}{1-\upsilon}\mu \quad , \tag{2.7}$$

in which, υ is Poisson's ratio and μ is the shear modulus of the metallic glass.

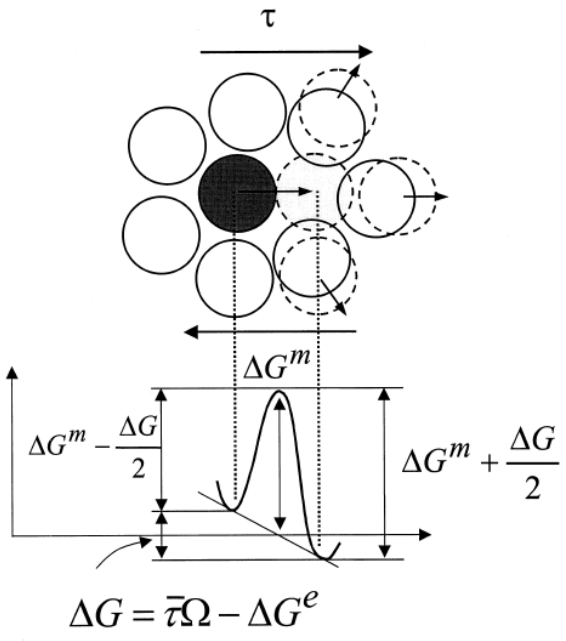

Fig. 2.3 A schematic of an individual shear event envisioned by Spaepen [68].

Following Spaepen, Argon [8] assumed that the diffusion-like flow behavior mechanism in metallic glass involves a process of stress-induced cooperative rearrangement of small groups of atoms called the "shear transformation zone (STZ)". As discussed above, the shear localization process is generally a result of work softening. Argon modeled this localization from the perspective of free volume theory and connected the shear banding behavior with the free volume accumulation as well as the related structural evolution through rationalization from the STZ model. The STZ model involves the movements of a group of

atoms rather than a single atom and these shear transformation zones can connect with each other to accommodate the applied shear stress, which can accordingly produce the so-called "shear bands". In this light, it can be seen that the amount of free volume can directly affect the shear band formation process and thus play an effect on the macroscopic ductility of the metallic glasses. Furthermore, it has been found that the free volume can behave as the beneficial site to initiate or even bifurcate the shear bands and hence improve the plasticity of BMGs [82, 83]. This close relationship between the free volume and shear band operation has offered a convenient avenue to toughen BMGs. Up to now, most scientists have been interpreting their works using the free volume model proposed by Spaepen and the STZ model developed by Argon.

2.4 Review of Development of Toughening BMGs

Since the birth of BMGs and the recognization of the problem of their brittleness, studies on enhancing the ductility of BMGs have being carried out widely, and up to date, many intrinsic and extrinsic methods have been developed to improving the plastic deformability of BMGs. These proposed strategies include fabrication of bulk metallic glass matrix composites, increasing Poisson's ratio, decreasing sample size, designing geometric confinement, testing conditions optimization. In what follows, a review of them will be performed one by one in detail.

2.4.1 In-situ/Ex-situ fabrication of metallic glass composites reinforced with crystalline phases

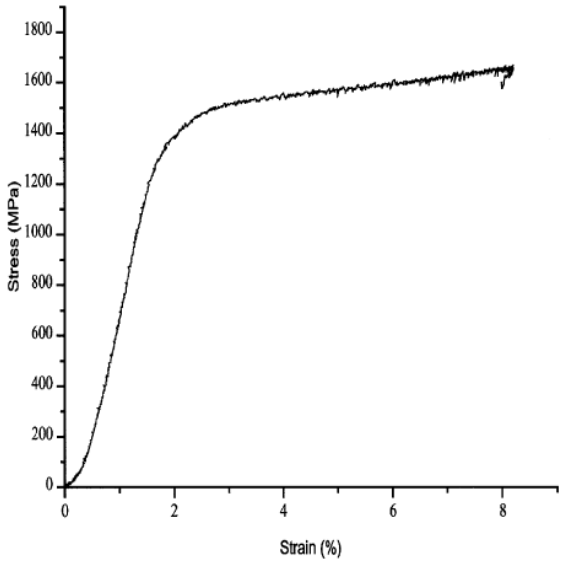

Fig. 2.4 Compressive stress strain curve for cylindrical in situ composite specimen [84].

To overcome the catastrophic failure of BMGs under unconstrained loadings, synthesis of BMG matrix composites has been widely recognized as the most promising way to engineering metallic glasses as structural materials. In principle, BMG matrix composites can be classified into two categories: in-situ composites and ex-situ composites. In in-situ composites, the metallic glass matrix is reinforced with secondary dendritic phases, which are produced in the form of precipitates during continuous casting. In the case of ex-situ composites, metallic particles (e.g. WC) or metallic fibers (e.g. Mo, W, Ta, and stainless steels) are introduced into the metallic glass matrix in the process of solidification of the metallic glass liquids. The ductile secondary crystalline phases, i.e., the metallic

dendritics, fibers or particles can assist in inhibiting the rapid propagation of shear bands, thereby enhancing the global ductility of the metallic glass. Take a Zr-based in-situ BMG composite as an example [84], the introduction of ductile crystalline Ti-Zr-Nb phase into the metallic glass matrix can remarkably increase the macroscopic plasticity and the resulting BMG composite can sustain a plastic strain of around 6% prior to failure as shown in Fig. 2.4.

2.4.2 Heterogeneous structure

Recent studies identified that introduction of heterogeneous structure into BMGs is an effective approach to toughen BMGs. This heterogeneous structure can be formed by means of phase separation [85-89]. In some glass forming systems, liquid phase separation can easily occur if the constitutional elements have repulsive interactions [90]. For instance, Pan *et al* [88] successfully enhanced the plasticity of a $Cu_{46}Zr_{47}Al_7$ BMG by substituting Cu with *at.* 1% Fe to get a $Cu_{45}Zr_{47}Al_7Fe_1$ BMG, in which a Cu-rich phase and an Fe-rich phase were formed. In the phase-separated heterogeneous structure, different domains in the BMGs hold different chemical compositions and different packing densities, giving rise to different moduli and different critical shear stresses [85]. Consequently, the propagation of the preferentially initiated shear bands that might nucleate at the softer phase sites can be hindered by the harder phase with a higher critical shear stress, which in turn activates other preferential sites for shear band formation. Accordingly, the heterogeneous structure is able to hinder

the propagation of shear bands as well as promote multiple shear bands activation, and thus improve the macroscopic plasticity. Even without the occurrence of liquid phase separation during solidification, heterogeneous structure may also be acquired. Liu *et al* [146] observed a group of super plastic (more than 160% true strain) ZrAlNiCu BMGs in which dispersive "soft" regions were surrounded by "hard" regions but no phase separation was evidenced. In a similar manner, the soft regions in this inhomogeneous structure provide preferential sites for shear band nucleation, while the hard regions impede the shear band propagation, alter the propagation orientations and assist the multiplication of shear bands.

Additionally, it is noticeable that the chemical heterogeneity in the BMGs may not only contribute to the plastic strain, but also render the BMGs "work-hardenable" during compressive deformation [88, 91, 92]. This "work-hardening" behavior is probably due to the continuous activation of multiple shear bands in succession at different regions possessing different critical shear stresses as well as the intersection of shear bands induced increase in flow stress. However, this work hardening ability and the plastic character of the BMGs with structural heterogeneities are closely linked with the morphology and the distribution of the chemically inhomogeneous domains within the BMGs.

2.4.3 Martensitic transformation mediated ductility enhancement

It is well known that the crystalline CuZr phase is rather ductile and can undergo a reversible martensitic transformation from B2 phase to B19' phase upon deformation, making the CuZr-based alloys not only work-hardenable but also shape memory [93-96]. Following this line of thought, Pauly *et al* [97-100] and Wu *et al* [101, 102] also discovered martensitic transformation mediated work-hardening and ductility enhancement in CuZr-based BMGs under both compressive and tensile loadings. It has been reported that the crystalline phase that favorably nucleates or precipitates in the solidification of Cu-Zr-Al ternary metallic glass alloys is metastable B2 CuZr phase since this phase crystallizes polymorphically while precipitation of other equilibrium phases like $Cu_{10}Zr_7$ necessitates long distance diffusion [103-105]. Fig. 2.5 and Fig. 2.6 are two cross-sectional photographs of the as-cast Cu-Zr-Al BMGs containing B2 CuZr phases embedded in the amorphous matrix [99, 100]. As shown in Fig. 2.5, sparse nanocrystals with diameters of 2-5 nm can be detected in some regions of a $Cu_{47.5}Zr_{47.5}Al_5$ BMG and electron diffraction identifies that these nanocrystals are B2 CuZr phase. While in a $Cu_{46}Zr_{46}Al_8$ BMG as displayed in Fig 2.6, the cloud-like contrast may arise from the structural heterogeneity. The electron diffraction in the left inset shows no presence of crystalline phases. But high magnification scattered lattice fringes with diameters of 2-5 nm are obviously visible in the right inset. Fast Fourier Transformation (FFT)-filtered image analysis identifies these ordered regions to be B2 CuZr phase. In fact, the B2 CuZr phase embedded within BMGs may increasingly precipitate and grow due

to a decrease in instantaneous shear modulus during mechanical deformation [100]. This precipitation process competes with the initiation of shear bands and hence shear banding process can be postponed. When the instantaneous shear modulus is softened to a certain level during mechanical loading, the metastable B2 CuZr phase twins and evolves into B19' CuZr phase (i.e., martensitic phase transformation takes place) as shown in Fig. 2.7, which is the low-resolution TEM micrograph of a $Cu_{47.5}Zr_{47.5}Al_5$ BMG after fracture, revealing an abundance of nanocrystals with sizes ranging from 10 nm to 50 nm [100]. Some of these nanocrystals show a diffraction contrast typical of nanotwins. This interesting deformation procedure is proposed to be understood based on the potential energy landscape concept. The continuous precipitation of B2 CuZr phase and the subsequent martensitic transformation from B2 CuZr phase to B19' phase assist release the stress concentration in the amorphous matrix and restrict the accumulation of free volume, thus postponing the initiation of shear bands and retarding the rapid propagation of shear bands [106]. In turn, the ductility of BMGs is highly improved and also further stress is required to move the shear bands during deformation, resulting in a work-hardening effect. This transformation induced plasticity effect arises in many shape memory alloys [107].

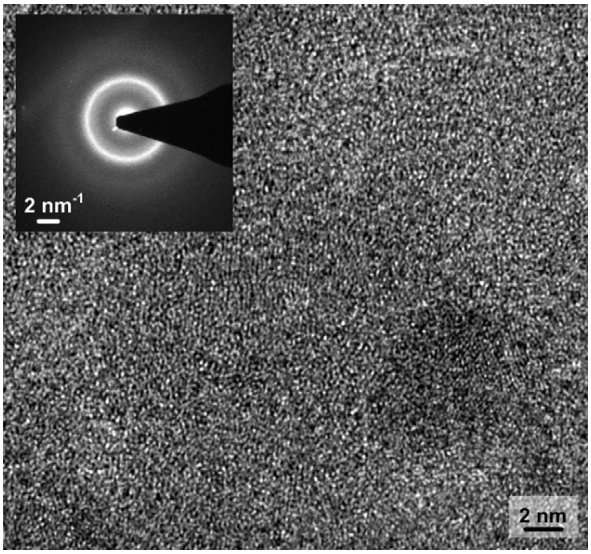

Fig. 2.5 TEM micrograph of an as-cast $Cu_{47.5}Zr_{47.5}Al_5$ BMG. The left inset is the corresponding electron diffraction pattern [99].

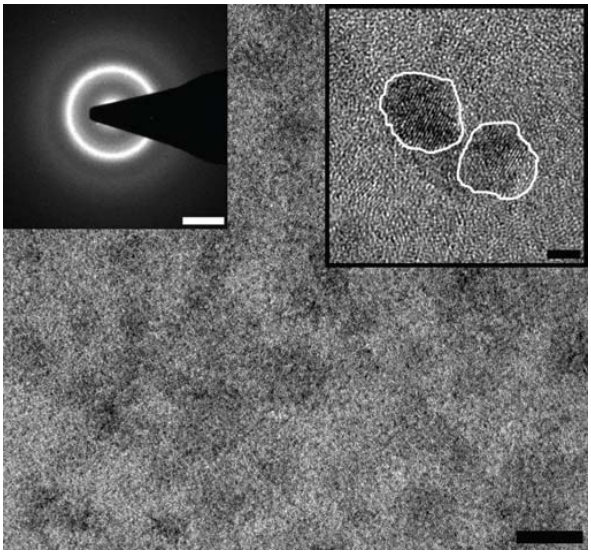

Fig. 2.6 TEM micrograph of an as-cast $Cu_{46}Zr_{46}Al_8$ BMG. The left inset is the corresponding electron diffraction pattern and the right inset shows the high magnification scattered lattice fringes [100].

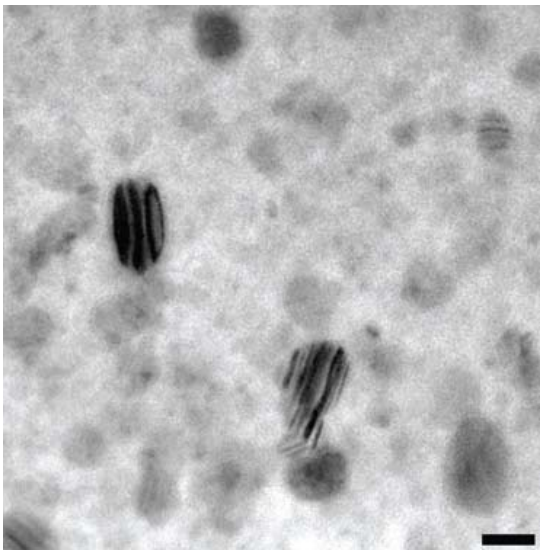

Fig. 2.7 Low-resolution TEM micrograph of a $Cu_{47.5}Zr_{47.5}Al_5$ BMG after fracture [100].

2.4.4 Increasing Poisson's ratio

By summarizing a huge number of data tested on a variety of BMGs, Lewandowski *et al* [108] firstly reported a close connection between the intrinsic plasticity of BMGs and the Poisson's ratio, υ, and put forward a rule that the larger the Poisson's ratio, the more ductile the BMG. Furthermore, an empirical critical value of Poisson's ratio $\upsilon > 0.31$-0.32 can usually guarantee a certain measure of plasticity, which has been confirmed in a series of BMGs [109, 110]. Generally, the Poisson's ratio can be controlled by tailoring the chemical composition. For instance, Yu *et al* [111] found that the plasticity of a $(Cu_{50}Zr_{50})_{100-x}Al_x$ (x = 0-10) BMG varied dramatically with the fluctuation of Al content as shown in Fig. 2.8. The homologous relation between the plastic strain and Poisson's ratio provides a direct insight into the plasticity of BMGs and should be helpful for designing more ductile BMGs through adjustment of the

chemical composition.

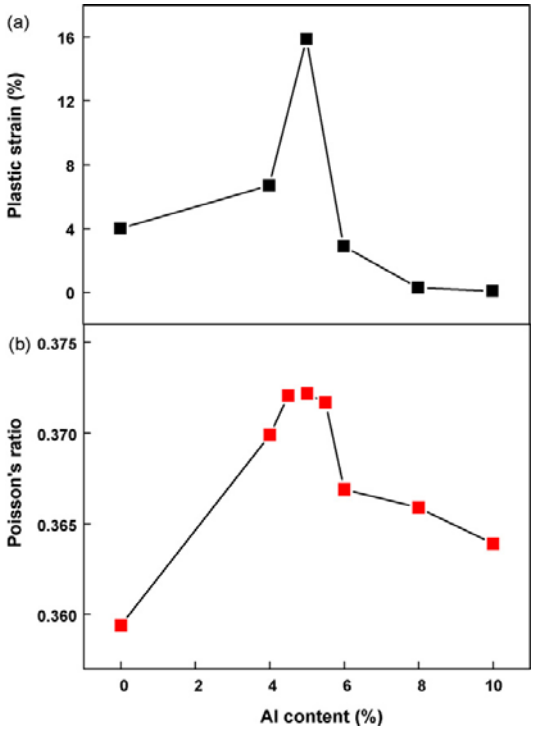

Fig. 2.8 The dependence of plastic strain and Poisson's ratio on Al content for the $(Cu_{50}Zr_{50})_{100-x}Al_x$ (x=0, 4, 5, 6, 8) BMGs [111].

As for the underlying mechanism controlling the plasticity of BMGs by Poisson's ratio υ (or the ratio of shear modulus μ to bulk modulus B, μ/B), Schroers and Johnson *et al* [109, 112] interpreted it in light of a competition between shear and dilatation: a small μ suggests an inferior ability of resisting shear plastic deformation, while a large B reflects in a strong capability in resisting dilatation required for mode I crack propagation. A high Poisson's ratio (above 0.31 ~ 0.32) tends to cause the tip of a shear band to extend forward rather than to initiate a crack [109]. This seems in great resemblance to the correlation of these two variables in crystalline solids as a competition between plastic flow and fracture proposed by Kelly *et al* [113].

2.4.5 Size effect

Size effect on mechanical behavior of conventional crystalline materials has been extensively studied [114, 115]. However, due to the limited amount of investigations on BMGs, size effect in BMGs is still a controversy, especially when some abnormal findings have been reported. To illustrate, it is well known that BMGs always exhibit nearly no tensile plasticity, but an investigation of tensile deformation of a metallic glass micropillar at the sub-micron size showed that this micropillar could undergo a large tensile plastic strain ranging from 23% to 45% involving significant uniform elongation and even extensive necking or stable growth of the shear offset [116]. The large tensile plasticity achieved in the micropillar metallic glass is believed not to originate from the branching or deflection of shear bands or nanocrystallization during deformation but through a deformation manner/mechanism similar to its crystalline counterparts, i.e., homogeneous (uniform elongation) and inhomogeneous (necking or stable growth of the shear offset) flow without catastrophic failure. Volkert *et al* [117] also conducted an array of uniaxial compression tests on PdSi metallic glasses columns with diameters ranging from 140 nm to 8 μm and found that the columns with diameters larger than 400 nm exhibited shear band formation process on a plane at 50° to the loading axis after elastic deformation while the columns with diameters lower than 400 nm showed a totally distinct deformation mechanism, i.e., homogeneous deformation followed by elastic behavior. The difference in plastic deformation mechanism with variation of sample size has

been attributed to a required critical strained volume for shear band formation. In this sense, since BMGs can be expected to display larger ductility if the shear band formation can be circumvented in small scaled specimens, this sample size effect discovered may be an implication for designing more ductile metallic glasses utilized in thin film or micro-device technology, which can assist in understanding the size effect in mechanical responses of metallic glasses as well [118].

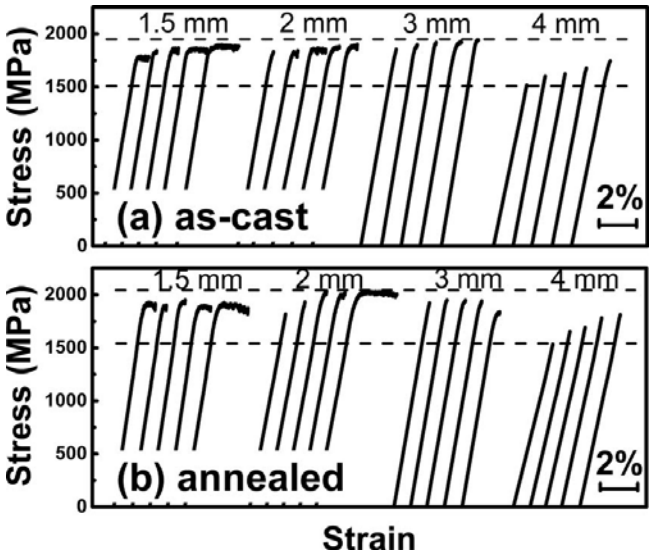

Fig. 2.9 Stress-strain curves of $Zr_{48}Cu_{45}Al_7$ with different sizes under compression: (a) as-cast and (b) annealed samples [119].

Even at a much larger size, millimeter sclae, size dependent ductility has also been reported in a Zr-based BMG, which displays a "malleable-to-brittle" transition at a critical sample size of 3 mm in diameter [119]. It was found that for the samples tested below the critical size of 3 mm (1.5 mm and 2 mm) in diameter, they exhibited nearly consistent strength with certain plastic strains before failure, but for the other group of specimens of 3 mm and 4 mm in

diameter, they almost failed in a quite brittle manner and displayed smaller strength than the former ones, as shown in Fig. 2.9(a). Worthy to note is that in the annealed samples, in which the free volume had been almost annihilated out, the similar "malleable-to-brittle" transition tendency was also discovered [shown in Fig. 2.9(b)]. Having eliminated the role of free volume in the size effect of mechanical properties of BMGs by means of annealing, this "malleable-to-brittle" transition phenomenon was explained in terms of geometrical "sample size effect" proposed by Ashby *et al* [120], who assumed that if the sample size was larger than the critical plastic zone size of the material, then brittle fracture would overwhelm the plastic flow and thus brittle fracture would follow. Furthermore, the decrease in strength for BMGs with diameters larger than critical plastic zone size could be understood in terms of defect concentration sensitivity, which had been also rationalized previously [121].

2.4.6 Geometric confinement

In recent years, it has been found that geometric confinement can be successfully employed to improve the room temperature plasticity of BMGs. For instance, Yu *et al* [15] reported that the plasticity of a $Zr_{41.2}Ti_{13.8}Cu_{12.5}Ni_{10}Be_{22.5}$ (Vit-1) BMG can be enhanced from ~0.5% to ~8% by a copper shrink-fit sleeve. Likewise, an increase of plasticity has also been accomplished in a $Zr_{58}Ni_{13.6}Cu_{18}Al_{10.4}$ metallic glass by virtue of an electrodeposited nanocrystalline Ni-15%Fe coating [16]. Most recently, Choi *et al* [17] enhanced the plasticity of Vit-1 BMG through

electrodepositing a copper coating onto it and they built a schematic model to describe a plastic deformation region ("crack buffer zone"), where the elastic energy stored in the BMG during loading can be released and absorbed as plastic deformation energy of the outer soft layer of Cu coating, thereby delaying the propagation of shear bands and promoting the proliferation of shear bands, as shown in Fig. 2.10.

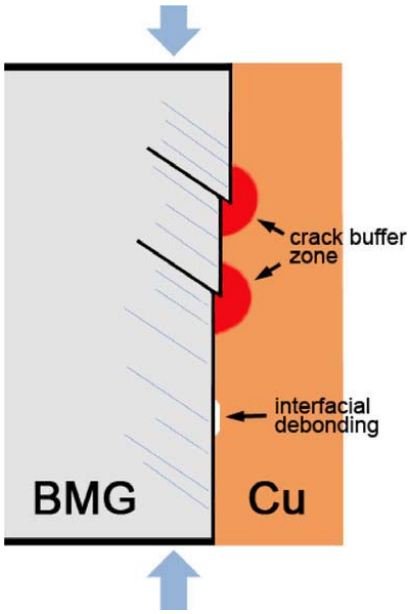

Fig. 2.10 Schematic drawing showing the plastic deformation region, in which the elastic energy release is absorbed as plastic deformation [17].

In fact, before these investigations, Lu *et al* [122] has already performed lateral geometric confinement by means of inserting a cylindrical BMG specimen into the cavity of a hollow cylinder (shown in Fig. 2.11), and studied this effect on the compressive properties of the BMG. They systematically evaluated the radial confining stress using a number of quantitative equations. During the elastic deformation regime for both of the BMG and sleeve, the confining stress

imposed on the BMG by the sleeve can be estimated by

$$\sigma_c = \frac{\sigma \nu_B / E_B}{\left(\frac{b^2 + a^2}{b^2 - a^2} + \nu_c\right) / E_c + (1 - \nu_B) / E_B}, \quad (2.8)$$

in which σ is the loading stress along the axial direction, E_B and E_c denote Young's modulus of the BMG and coating, respectively; a is the inner diameter of the coating or the diameter of the BMG rod, b is the outer diameter of the coating. However, due to the much higher yield strength of BMG than the outer sleeve (stainless steel) they chose, the confining stress should be estimated according to equation (2.9) as follows when the sleeve begins to yield while the BMG still experiences elastic deformation:

$$\sigma_c = \sigma_s [\ln \frac{\rho}{a} + \frac{1}{2}(1 - \frac{\rho^2}{b^2})], \quad (2.9)$$

where σ_s is the yield stress of the sleeve, ρ represents the radial location where the sleeve starts to yield (elastic-plastic boundary), a variable correlated with the hoop strain at the outer surface of the sleeve, Young's modulus and yield strength of the sleeve as well. Based on the above functions, Lu *et al* [122] found that the the compressive plastic strain was shown to increase with increasing the confining stress by enhancing the thickness and the yield strength of the outer sleeve. Hence, a direct relationship between the intrinsic yield strength of the confining sleeve and the plasticity of the BMGs can be rationalized. The stronger the confining sleeve is, the more plastic the BMGs will be, provided that the bonding at the BMG/sleeve interface is strong enough.

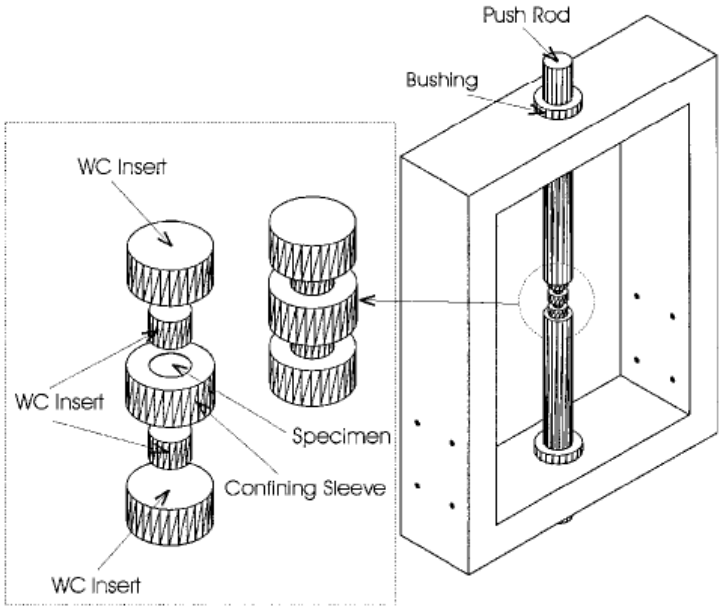

Fig. 2.11 Quasistatic compression fixture and the radial confinement apparatus [122].

2.4.7 Testing conditions

Some investigations suggested that the mechanical properties of BMGs are also quite sensitive to testing conditions including testing temperature [123, 124], strain rate [125-134], stiffness of the testing machine [135], or even the mechanical testing boundary conditions [13]. Therefore, it is feasible to obtain enhanced plasticity of BMGs from the perspective of optimizing the testing conditions or modulating the serving conditions when in practice.

Li *et al* [123, 124] studied the compressive response of a Zr-based BMG at room temperature and liquid nitrogen temperature, respectively, and found differences in strength and ductility exhibited by the same BMG sample, as shown in Fig.

2.12. The origin for this phenomenon is thought to be the decreased mobility of free volume with the decrease of ambient temperature. When the mobility of free volume is impaired at cryogenic temperature, the initiation of shear band will be delayed since shear band development is a thermally activated process [136-138]. Meanwhile, with the decreased temperature ahead of the shear band tip and within the shear band, the propagation of the shear band will also become more difficult. Thus, the plasticity of BMGs can be improved and a higher load is required to launch the shear localization.

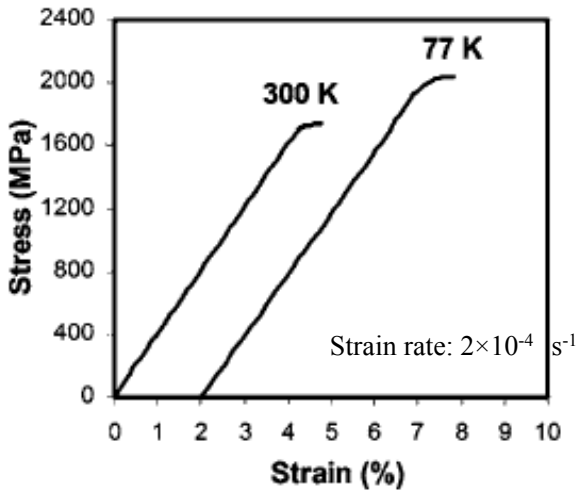

Fig. 2.12 Compressive stress-strain curves of the $Zr_{57.4}Ni_{13.4}Cu_{17.9}Al_{10.3}Nb_1$ metallic glass at room temperature 300 K and liquid nitrogen temperature 77 K [124].

Strain rate-dependent behavior has been discovered in many BMGs during various mechanical testing conditions including fracture toughness testing, nanoindentation testing, uniaxial compressive and tensile testings. For instance, Hufnagel *et al* [126] found in a metallic glass that the fracture stress decreased

with increasing loading rate during uniaxial quasi-static compression. Kawamura *et al* [127] observed a loss of tensile strength of a rapidly solidified $Zr_{65}Al_{10}Ni_{10}Cu_{15}$ amorphous ribbon with the increment of strain rate. Furthermore, Mukai *et al* [128] discovered that the shear band density generated in a Pd-based BMG rised with the growth of strain rate under tensile loading, manifesting that strain rate not only influenced the tensile/compressive fracture strength but had an important influence on the process of shear band formation in BMGs as well, which was also corroborated by nanoindentation and fracture toughness investigations [125, 136-138]. In sharp contrast, Bruck *et a*l [139] and Lu *et al* [140] both pointed out that the dynamic compressive failure stress of BMGs was independent of testing strain rate. Analyzing available experimental results, the mechanical behavior under different strain rates seems significantly controlled by many factors, involving the degree of amorphization, loading mode, and chemical compositions of BMGs [141]. However, it has been widely recognized that at low strain rates, a single shear band operates to accommodate the applied strain swiftly, whereas at high strain rates, a single shear band cannot catch up with the applied strain. Consequently, even when the first shear band is formed, stress cannot be released in the surrounding matrix in a timely manner but the yield condition remains satisfied in other regions, leading to the activation of multiple shear banding events in different locations to accommodate the applied strain [77].

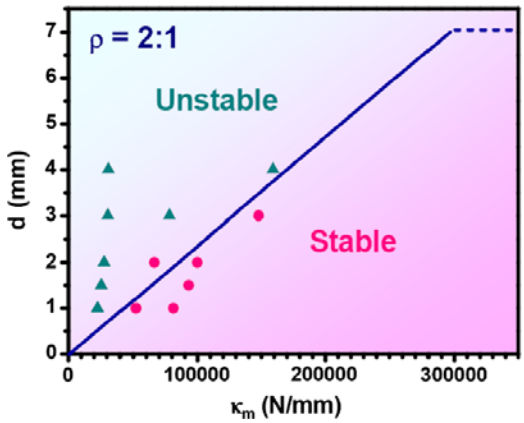

Fig. 2.13 A stability/instability map with respect to the sample size d and machine stiffness K_m for samples of aspect ratio = 2:1 [135].

Han *et al* [135] found that the plasticity of BMGs strongly depended on the stiffness of the testing machine and firstly derived an instability index for shear-band failure in BMGs from the standpoint of free energy changes in the sample-machine system. They described an instability/stability map (shown in Fig. 2.13), which could identify a critical transition from instability to stability as a function of sample size and machine stiffness. Herein, the stability is interpreted as the simultaneous operation of multiple shear bands, corresponding to a notable plasticity, while the instability can be illustrated as the operation of a single dominant shear band, corresponding to a limited plasticity. For a certain sized BMG sample, this instability index incorporates the effect of stiffness of the testing machine into the mechanical response of BMGs and can thus provide a guide for setting serving conditions, under which plastic deformability can be obtained for BMGs.

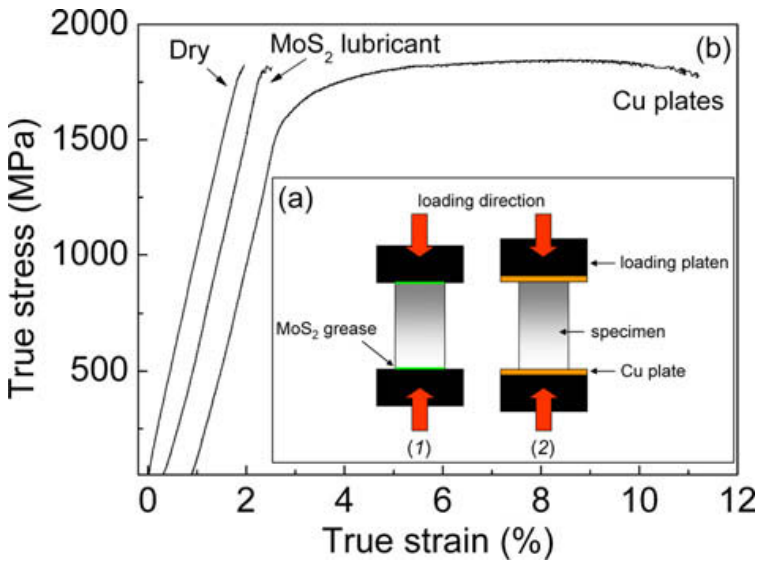

Fig. 2.14 (a) Schematic illustration of the boundary conditions used for the compression tests and (b) true compressive stress-true strain curves for the Vit1 BMGs tested in dry loading conditions, MoS_2 grease lubricated loading condition and Cu plates lubricated loading condition [13].

Most recently, an investigation made by Scudino *et al* [13] indicated that the mechanical response of BMGs is also closely correlated with the boundary conditions during testing. Under compressive loading, which is the most popular testing method for mechanical evaluation of BMGs, weaker friction at the interfaces between the loading platens and test specimen achieved by lubrication can alter the mechanical behavior of BMGs, and effectively enhance the macroscopic plasticity of BMGs as shown in Fig. 2.14. As for the reason, due to the elastic mismatch between the specimen and the loading platens, frictional boundary restraints can arise at the interfaces, which suppress the lateral spreading of the material on the ends (i.e, so-called "clamping" effect) [142-144]. However, if a lubricant such as a Cu foil is inserted at each loading interface, the

friction at each end of the test sample can be reduced considerably, as evidenced by previous studies [145]. In addition, it should be pointed out that the soft Cu foils inserted at the interfaces can also exert a lateral pressure near the edges of the material and help the lateral spreading of the BMG instead.

Chapter 3 Experimental Procedures

3.1 Materials and specimen preparations

The BMG specimens studied in this work are selected from two families of BMGs, i.e., Zr-based $Zr_{57}Al_{10}Ni_8Cu_{20}Ti_5$ (*at.* %) and Fe-based $Fe_{75}Mo_5(P_{50}C_{41.67}B_{8.33})_{20}$ (*at.* %) BMGs. The reason for selecting these two BMGs is that Zr-based BMGs typically have a strong glass forming ability, which suggests a great potential to be widely used as engineering structural materials in the future. While among the existing numerous BMG systems discovered, Fe-based BMGs are known to possess great commercial potential due to their superior magnetic properties, ultrahigh strength as well as low material cost, as mentioned earlier, though they are disappointingly brittle. In this sense, it is very practically significant to improve the plasticity of Fe-based BMGs, especially given that the recent achievements in this field have indeed provided a promising light for getting more ductile Fe-based BMGs [146, 147].

Under a titanium-gettered argon atmosphere, the master alloy ingots with nominal composition of $Fe_{75}Mo_5(P_{50}C_{41.67}B_{8.33})_{20}$ for Fe-based BMG were prepared by the arc-melting of a mixture of pure Fe (99.9%), Mo (99.9%), C (99.999%), B (99.95%) and industrially used Fe-P alloy composed of 72.6% Fe, 25.3% P and other impurities, while the master alloy ingots of $Zr_{57}Al_{10}Ni_8Cu_{20}Ti_5$ metallic glass were also prepared by arc-melting the pure elements together. Each

Zr-based and Fe-based ingot was then remelted at least five times to ensure a homogeneous composition. After this, Fe-based BMG rods of diameter 1.5 mm and Zr-based BMG rods of diameter 2 mm were produced by copper mould suction casting.

3.2 Metal electroplating

Metal electroplating is often a means of producing a surface coating that possesses some properties superior to those of the substrate materials, thus extending the use of substrate materials to more fields of application [148]. Cu and Ni plating are well known so far as two of the most common metal electrodeposition technologies for a wide range of industrial applications. It should be noted that electroplating is not just a simple dip and dunk procedure. Instead, electroplating involves a lot of critical elementary phenomena (e.g., surface phenomena) and process steps such as solid state processes and processes in the liquid state [149]. Regularly, many factors can influence the process of metal plating. These factors includes the orientation of the substrate, the temperature of the electrolyte solution, the composition of the electrolyte solution, the plating time, the current density and so forth [29]. During the experiments in the current work, except for the electroplating time for achieving different thicknesses in some cases, all other electroplating parameters were maintained constant, guaranteeing an identical plating environment and repeatably good resulting coating properties.

3.2.1 Cu electroplating

A common copper sulphate-sulfuric acid bath was used for the Cu coating deposition. The electroplating solution was prepared from cupric sulfate pentahydrate and reagent 98 wt. % pure grade sulfuric acid to obtain an electrolyte with a concentration of 64 g/L copper ion and 73.5 g/L sulfuric acid. A electroplating specimen used polycrystalline copper-phosphorous plate containing around 0.1 wt. % phosphorous and was adopted as the anode. Behaving as the cathode, the BMG rod was vertically placed into the electrolyte about 30 mm away from but parallel to the anode. It is worth mentioning that prior to electroplating, the surface of all the BMGs were mechanically ground and carefully polished to make them as smooth as possible, followed by degreasing and rinsing in deionized water. More importantly, for the two end coated and completely encapsulated BMGs, cylindrical rods with an aspect ratio of 2:1 were all cut by a low speed diamond saw and both ends of the specimens were polished carefully to ensure parallelism and perpendicularity prior to electroplating because of the standard requirement of the uniaxial compression tests. In addition, a relatively small current density of 0.2 mA/mm^2 ± 0.01 mA/mm^2 was chosen for Cu electroplating at room temperature. In order to ensure an evenly distributed Cu coating, the BMG rods were continuously rotated by a motor at a constant speed of 50 r/min. Also, magnetic agitation was employed to avoid the occurrence of an inhomogeneous electrolyte.

3.2.2 Ni electroplating

A traditional aqueous Watts electrolyte containing nickel sulphate, nickel chloride and boric acid was prepared for Ni coating electroplating, as described in Ref. [150]. A piece of pure Ni sheet (99.99%) was utilized as the anode while the BMG rod acted as the cathode. Before Ni electroplating, the surface of all the BMG specimens were polished carefully to ensure smoothness and purity according to the procedures that have been described above in the Cu electroplating process. Ni electroplating was carried out under a current density of approximately 0.1 mA/mm^2 at room temperature. The distance between the anode and the cathode was fixed at 30 mm. During the process of Ni electroplating, the BMG rod was rotated by a motor at a constant speed of 50 r/min to produce an even Ni coating. Meanwhile, gentle magnetic stirring was maintained to ensure a homogeneous solution for electrodeposition.

3.2.3 Cu/Ni dual bath electroplating

According to the conceptually simple dual bath technique as shown in Fig. 3.1, akin to that described in Ref. [151], the acid sulphate solution and the aqueous Watts electrolyte were used for the two-step Cu plating and Ni plating, respectively. The details of the BMG pre-treatment and plating process have been introduced above. Note that after Cu electrodeposition, there were two cycles of water rinsing in deionized water, in which a second "water rinse 2" in a different beaker of deionized water aimed to completely get rid of the residual Cu plating

solution on the surface of the BMG rod. Rinsing in Ni electrolyte before Ni electroplating was performed to remove the water film remaining on the surface of the BMG rod, and also to guarantee the coverage of the BMG rod surface by a uniform layer of the Ni plating solution. Otherwise, if the BMG rod was transferred to the Ni plating electrolyte immediately after the water rinse, the water droplets adhering to the BMG may influence the application of electroplating current/voltage.

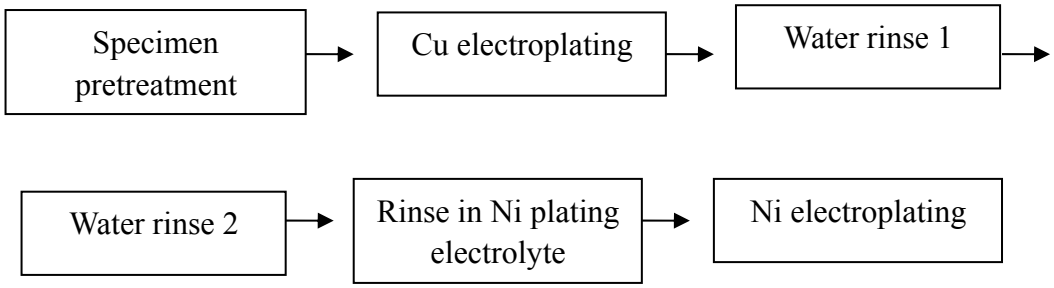

Fig. 3.1 Schematic diagram of the Cu/Ni two-step electrodeposition.

3.3 Structure characterization, thermal analysis and fracture morphology characterization

The amorphous structures of the BMG rod samples were all checked by conventional XRD with Cu-K_α radiation. XRD examinations were conducted through standard continuous scanning on a Bruker D8Advance X-ray diffractionmeter. The coating/BMG interfaces were observed using optical microscopy (OM) equipped with length scale measuring tools, which can measure the thickness of the outer coatings. In addition, a precision micrometer was utilized to measure the thickness of the coatings on either end of the

encapsulated Zr-based BMGs.

The thermal analysis was examined by DSC under a continuous flow of pure nitrogen gas. Temperature scanning was implemented continuously from room temperature to 520 °C (773K) for Zr-based BMGs and to 577 °C (850 K) for Fe-based BMGs, both at a heating rate of 20 K/min on a Perkin-Elmer DSC7 machine. The fracture morphologies of all the samples were observed by scanning electron microscopy (SEM) on a JEOL Model JSM-6490 machine.

3.4 Uniaxial Compression Tests

During compression at a constant strain rate, a BMG initially undergoes elastic deformation to the elastic limit, after which the structural defects such as a surface flaw or the residual free volume elicit the shear plastic deformation, i.e., serrated flow. As the shear bands in a BMG deform rapidly, the displacement rate of the material within the shear bands far exceeds that of the entire specimen, resulting in the drops of the applied load. In turn, when the load drops, the driving force for the shear band propagation is weakened, giving rise to the cesession of the shear band deformation. Hence, to further deform the BMG, a higher applied load is required. This load fluctuation process is well known as serrated flow. Consequently, uniaxial compression testing has been so far considered as one of the most common and convenient way to investigate the elastic deformation as well as the serrated flow behavior of BMGs.

In this work, uniaxial compression tests were conducted for various BMG samples. All the as-cast and coated BMG cylindrical specimens with an aspect ratio of 2:1 were tested in a uniaxial compressive deformation mode on a Materials Testing System (MTS) at room temperature with a quasistatic strain rate of 1×10^{-4} s^{-1}. A 10000 kg load cell in the MTS was fixed to measure the load. The strains exhibited by the specimens were all measured through an extensometer placed between two WC steel loading platens. To ensure repeatability, at least three compression tests were performed for each specimen.

3.5 Vickers hardness test

To determine the hardness evolution of the coated Zr-based BMGs after failure, hardness maps over a square of 1 × 1 mm were undertaken on the as-cast Zr-based BMG, the laterally coated Zr-based BMG, the two end coated Zr-based BMG and the completely encapsulated Zr-based BMG, before and after compressive deformation, utilizing a Mitutoyo hardness testing machine. Vickers indentations were performed each 100 μm (i.e. 100 dots measured for each specimen) with an applied load of 0.1 kg and dwell time 10 s before unloading.

3.6 Summary

The detailed BMG specimen preparation technique through Cu mold suction casting has been introduced in the beginning of this chapter. Whereafter, three different electroplating processes, i.e., pure Cu coating plating, pure Ni coating

plating and Cu/Ni bilayered coating plating were described. The details of the compression test performed on the MTS machine and the characterization techniques, primarily including XRD, DSC, SEM, Vickers harness test, were also presented in this chapter.

Chapter 4 Experimental Results: Structure and thermal behavior of as-cast BMGs

4.1 Amorphous structure of as-cast BMGs

Fig. 4.1 shows two sections through the as-quenched Fe-based BMG (left) and Zr-based BMG (right) sample of 1.5 mm diameter and 2 mm diameter, respectively. It can be seen from the figure that the Fe-based BMG sample contains considerably more casting defects, such as micro-pits on the surface, in comparison with the surface quality of the Zr-based BMG sample. This may be attributed to the more notable shrinking effect at the final stage in the smaller scale Fe-based BMG samples as well as the disparities in chemical composition and non-equilibrium solidification behavior between these two different BMG systems.

Fig. 4.1 Two sections of the as-cast Fe-based BMG (left) and Zr-based BMG (right) sample, respectively.

The representative XRD results shown in Fig. 4.2 confirm the amorphous structure of the Zr-based and Fe-based BMGs, with no evidence of crystalline diffraction peaks. The single broad peak in each figure indicates that both BMGs are of fully amorphous nature.

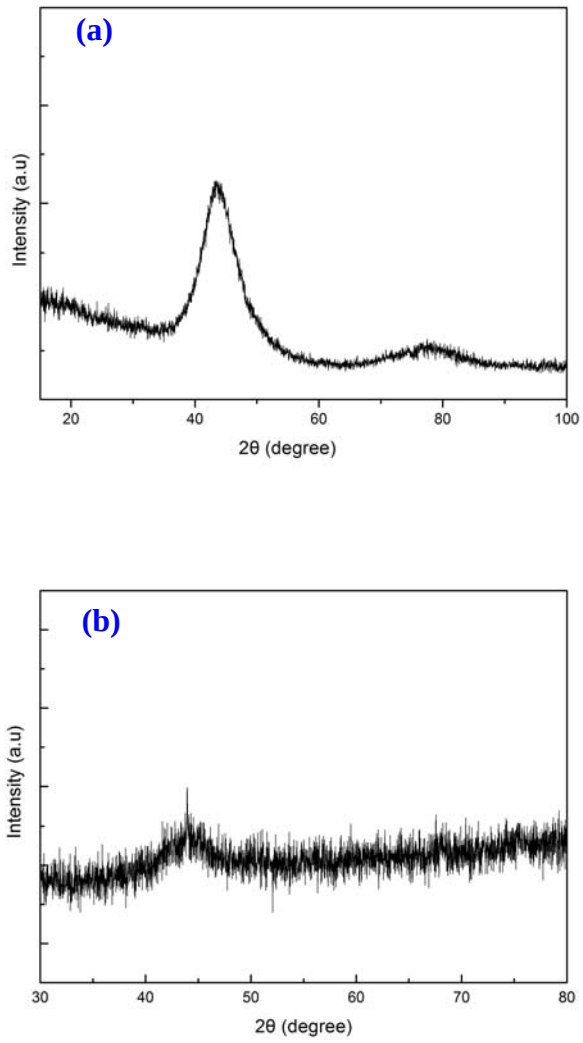

Fig. 4.2 Representative XRD patterns of the (a) Zr-based BMG and (b) Fe-based BMG.

4.2 Thermal behavior of as-cast BMGs

Fig. 4.3 shows the representative DSC curves of the two BMGs. A glass

transition interval can apparently be observed from each DSC curve. The glass transition onset temperature T_g and the crystallization onset temperature T_x for both BMGs are listed in Table 4.1. Here, it is found that a larger glass transition interval ΔT_x corresponds to a stronger glass forming ability if one compares the ΔT_x and the glass forming ability of the two BMGs selected in our work, which is very consistent with Inoue's empirical rule. For the $Zr_{57}Al_{10}Ni_8Cu_{20}Ti_5$ BMGs, fully amorphous rods of diameter up to 10 mm can be prepared by Cu mold casting [152] while for the $Fe_{75}Mo_5(P_{50}C_{41.67}B_{8.33})_{20}$ BMGs, rods of maximum diameter of only 3 mm with fully amorphous structure can be obtained by Cu mold casting [153], suggesting a notably weaker glass forming ability of the $Fe_{75}Mo_5(P_{50}C_{41.67}B_{8.33})_{20}$ BMGs. It should be noted that both of the two BMGs chosen in this work have more than only one single crystallization peak in their DSC curves, and the multi-step crystallization behavior upon heat-treatment may account for this multiple crystallization peaks behavior. Every crystallization peak that appeared in the DSC curve of a BMG corresponds to precipitation of a crystalline phase upon heating, so that the phenomenon of multiple exothermic peaks in the DSC curves is usually reflected in the multi-step crystallization behavior. Finally, the glass transition onset temperature T_g, to a large extent, has an intrinsic relationship with the value of shear modulus, which is a key parameter in determine the plasticity of BMGs [112, 154]. The higher the T_g, the larger the shear modulus, reflecting a larger activation energy is required for viscous flow [155], i.e., a larger T_g often poses a threat to the activation of shear

plastic deformation of BMGs. From this perspective, it is anticipated that the monolithic Fe-based BMGs are usually quite brittle in nature.

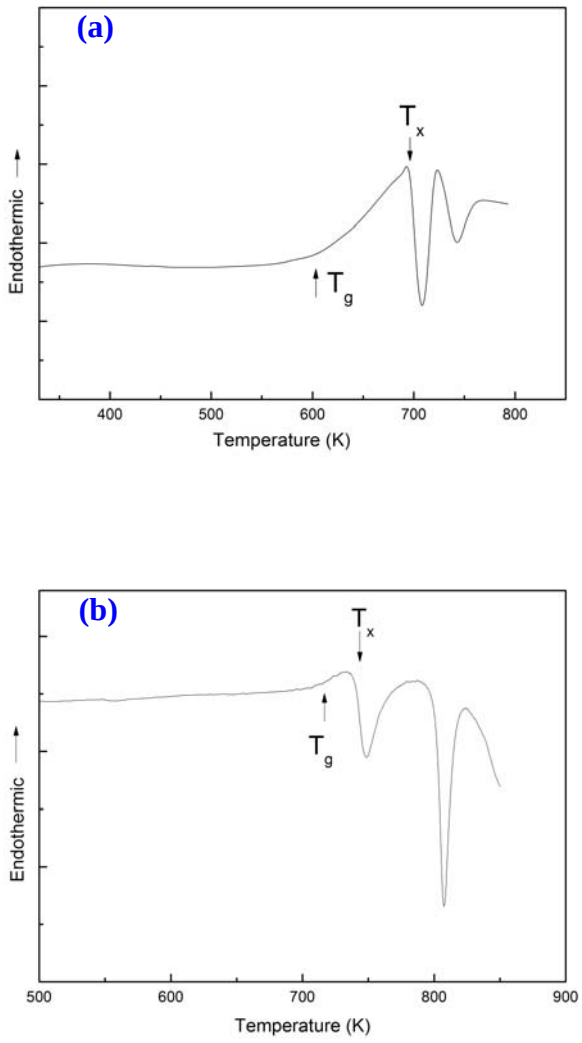

Fig. 4.3 Representative DSC curves of the (a) Zr-based BMG and (b) Fe-based BMG.

Table 4.1 T_g and T_x tested from the BMG samples.

Specimen	T_g	T_x
$Zr_{57}Al_{10}Ni_8Cu_{20}Ti_5$ BMG	605 K	698 K
$Fe_{75}Mo_5(P_{50}C_{41.67}B_{8.33})_{20}$ BMG	711 K	740 K

4.3 Summary

$Zr_{57}Al_{10}Ni_8Cu_{20}Ti_5$ BMG specimens and $Fe_{75}Mo_5(P_{50}C_{41.67}B_{8.33})_{20}$ BMG specimens were prepared by Cu mold suction casting and the profiles of the specimens were displayed. The fully amorphous microstructure of all the BMG samples was checked by the XRD pattern which showed a single broad peak with no crystalline diffraction peaks. The thermal behavior of the two BMGs was analyzed by DSC. In the DSC curves of the two BMGs, the glass transition temperature and the crystallization temperature were derived. Furthermore, the close link between the glass forming ability and the width of the superliquid liquid region ΔT_x proposed by Inoue was supported by the experimental results.

Chapter 5 Geometric coating confinement on the mechanical properties of BMGs

5.1 Improving plasticity of a Zr-based BMG by Ni plating

Fig. 5.1 shows the cross-sectional optical micrographs of the as-cast Zr-based BMG rod and the 76.6 μm Ni coated Zr-based BMG rod after Ni electroplated for about 3 hrs. From this figure, a good BMG/coating interface and an even distribution of Ni coating around the surface of the Zr-based BMG rod were observed.

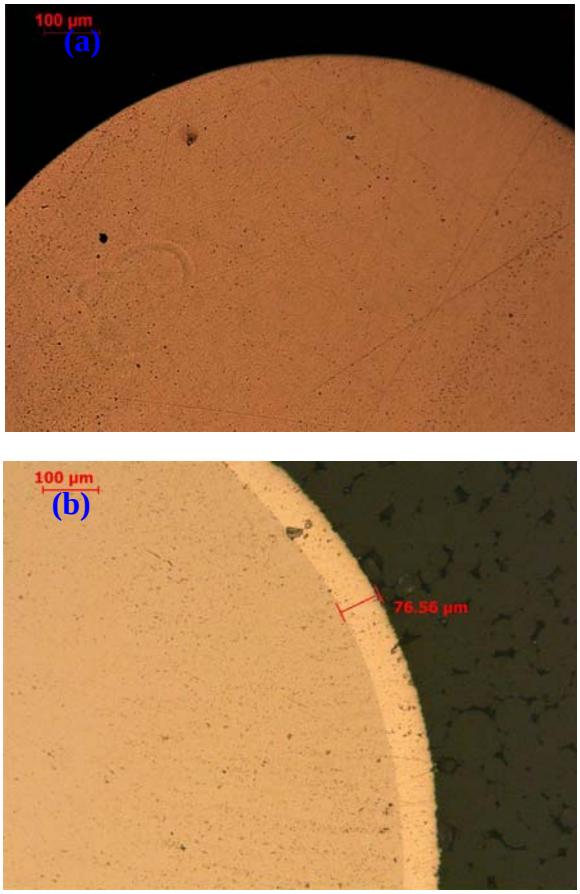

Fig. 5.1 Cross-sections of the (a) as-cast Zr-based BMG and (b) 76.6 μm Ni coated Zr-based BMG.

Fig. 5.2 plots the room-temperature engineering compressive stress-strain curves of the as-cast $Zr_{57}Al_{10}Ni_8Cu_{20}Ti_5$ BMG and the 76.6 μm Ni coated $Zr_{57}Al_{10}Ni_8Cu_{20}Ti_5$ BMG at a strain rate of 1×10^{-4} s^{-1}. Both specimens show serrations in the plastic region, which is a common trait for the mechanical response of BMGs under quasi-statistic uniaxial compression tests [156]. Moreover, the magnitude of the stress fluctuation in the serrations evolves from tiny through moderate to dramatic with the increase of the plastic strain. For those incipient tiny stress undulations, the elastic energy density is still below the threshold value for the shear band formation across the whole BMG, and thereby the external load cannot provide sufficient energy to propel the shear band to sweep across the entire cross-section of the sample [157]. For the moderate or larger stress undulations in the serration events, even the elastic energy density exceeds the critical value for the shear avalanche, the emanation of the branched secondary shear bands from the primary shear band can also consume a considerable proportion of the energy and delay the final instable catastrophic failure [157]. Thus, hunting avenues to absorb elastic deformation energy from a fundamental method to avoid the premature failure process and enhance the plasticity of BMGs.

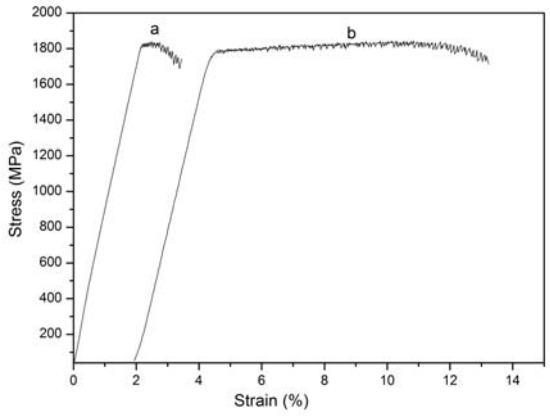

Fig. 5.2 The Uniaxial nominal compressive stress-strain curves of (a) as-cast Zr-based BMG and (b) 76.6 μm Ni coated Zr-based BMG.

From the compressive results, it was unambiguous that the coated Zr-based BMG exhibited a larger plastic strain than the uncoated one because of the lateral confinement by the Ni coating. The as-cast specimen was found to yield at 1807 MPa with a limited plastic strain of 1.3%. By contrast, the 76.6 μm Ni coated $Zr_{57}Al_{10}Ni_8Cu_{20}Ti_5$ BMG yielded at 1729 MPa with a plastic strain of 8.9% before failure.

In fact, the Ni coated BMG can be treated as a double layered composite. Since the thickness of the Ni coating is only a few % of the thickness of the composite, the contribution of the coating to the overall yield strength σ_y is negligible, according to the empirical "rule of mixtures" in the mechanics of composites [158].

$$\sigma_{\mathrm{y}} = \sigma_B V_B + \sigma_c V_c , \tag{5.1}$$

where σ_B and σ_C are the yield strengths of the BMG and Ni coating, respectively.

V_B and V_C are the volume fractions of the BMG and Ni coating, respectively. When substituting the yield strength σ_B = 1807 MPa and σ_C = 1000 MPa [29], and the volume fractions V_B = 91.7 % and V_C = 8.3 % into the above equation, it is found that the experimental results agree very well with the theoretical predictions.

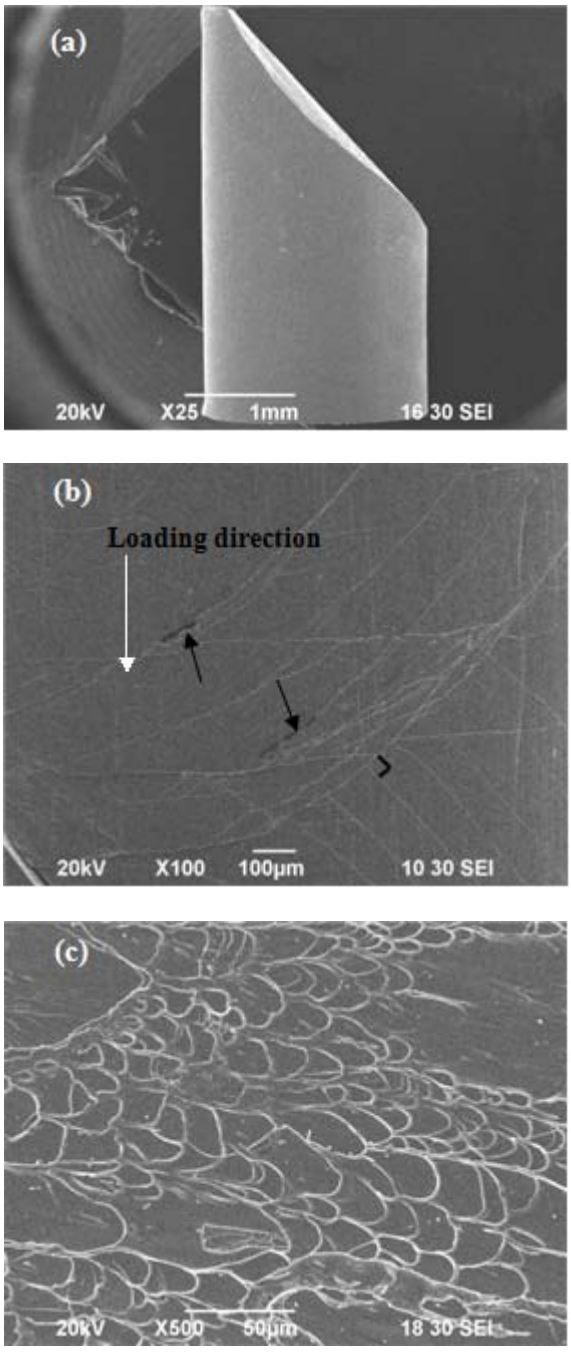

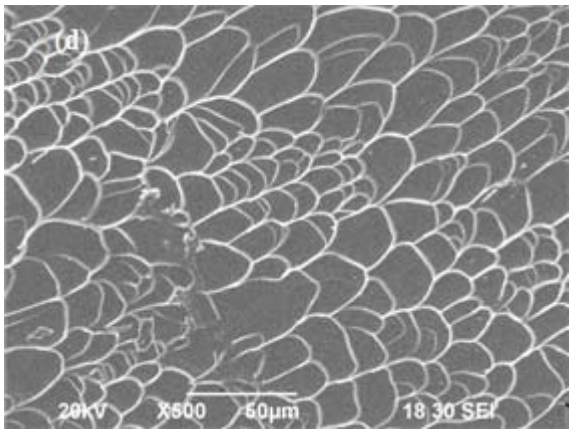

Fig. 5.3 (a) side surface view of the failed uncoated Zr-based BMG; (b) side surface view of the failed Ni coated Zr-based BMG; (c) a hybrid pattern on the fractured surface of the uncoated Zr-based BMG; (d) a hybrid pattern on the fractured surface of the Ni coated Zr-based BMG.

Fig. 5.3 displays the fracture morphologies of the uncoated Zr-based BMG and the Ni coated Zr-based BMG after failure. The number of shear bands on the side surfaces of the two failed specimens shown in Fig. 5.3(a) and (b) lent support to the compressive results. Clearly, many more shear bands appeared on the side surface of the coated sample compared with those on the uncoated one. The traces of shear bands were hardly discernible on the side surface of the uncoated specimen as shown in Fig. 5.3(a), and the majority of the limited macroscopic plastic strain of ~ 1% was probably achieved by the movement of the primary shear band, which evolved to the shear fractured plane after fracture. On the side surface of the Ni coated sample shown in Fig. 5.3(b), a large number of shear bands were detected. One can clearly find that besides a few shear bands in the horizontal direction, there are mainly two groups of parallel shear bands that are

perpendicular to each other, having an angle of nearly 45° with respective to the loading direction. These shear bands are highly branched and frequently intersect, showing wave-like passing patterns. Some of these shear bands become bent rather than extended straight and this can be attributed to the rotation mechanism during uniaxial compression tests [159]. As for the micro-cracks (marked by the arrows), they most probably originated from a tensile stress state led by coalescence and dilation of the free volumes within the shear bands [160]. It should be pointed out that the fractured shear planes of the uncoated Zr-based BMG and the Ni coated Zr-based BMG both exhibited a hybrid pattern, i.e., a vein pattern together with a river-like pattern as shown in Fig. 5.3(c) and (d), implicating a sort of similarity in the shear deformation mechanism before and after Ni electroplating. In fact, this hybrid pattern is a typical feature of the fracture morphology on the shear plane of many BMGs and it discloses an intermittent shear banding process along a shear plane direction as put forward by Spaepen [161]. In addition, many liquid-like droplets could be easily found on the shear planes of both specimens. It is believed that during localized plastic deformation, a substantial decrease in glass viscosity within the shear bands should have occurred, and can be attributed to the adiabatic heating and coalescence of the free volume [136, 162].

5.2 Improving plasticity of an Fe-based BMG by Ni plating

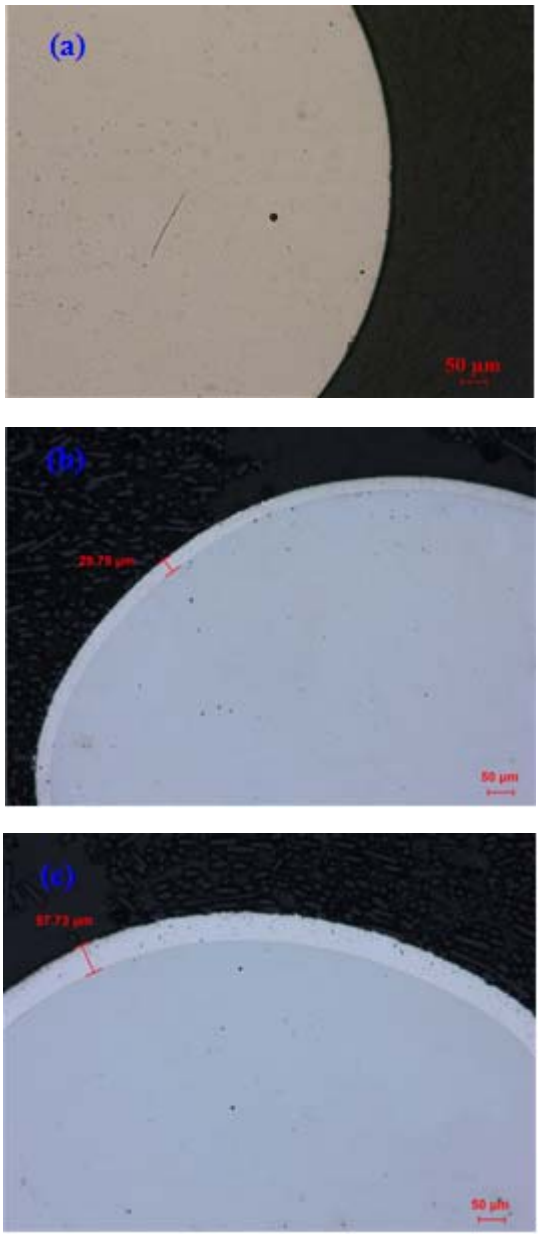

Fig. 5.4 Cross-sections of the (a) as-cast Fe-based BMG (b) 29.8 μm Ni coated Fe-based BMG; (c) 57.7 μm Ni coated Fe-based BMG.

As mentioned in Chapter 1, the ultrahigh strength Fe-based BMGs are usually far more brittle than other BMG systems, and exhibit a distinct fracture behavior. To clarify whether the geometric confinement by an electroplated metal coating is feasible for toughening these BMG systems, an $Fe_{75}Mo_5(P_{50}C_{41.67}B_{8.33})_{20}$ BMG

was selected in this work to be electroplated with two different thick Ni coatings, which could allow examinations of the influence of coating thickness on the geometric confinement effectiveness as well. Fig. 5.4 shows the representative optical micrographs of the cross-sections of the as-cast Fe-based BMG and the two Fe-based BMGs with different thick Ni coatings, 29.8 μm and 57.7 μm, corresponding to 2 hrs and 5 hrs electroplating time span respectively. From this figure, one can see a good interface between the Fe-based BMG and the Ni coating, and the homogeneous amorphous microstructure, without any obvious metallographical phase contrast.

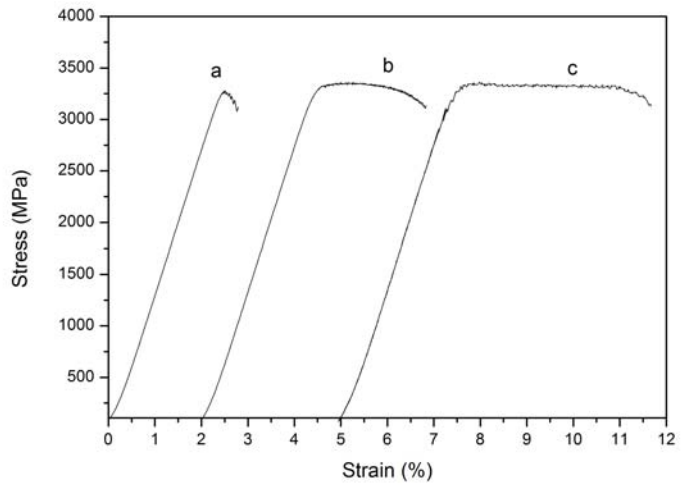

Fig. 5.5 The uniaxial nominal compressive stress-strain curves of the a) as-cast Fe-based BMG; b) 29.8 μm Ni coated Fe-based BMG; c) 57.7 μm Ni coated Fe-based BMG.

Fig. 5.5 plots the room-temperature uniaxial nominal compressive stress-strain curves of the uncoated $Fe_{75}Mo_5(P_{50}C_{41.67}B_{8.33})_{20}$ BMG and the two coated $Fe_{75}Mo_5(P_{50}C_{41.67}B_{8.33})_{20}$ BMGs, at a strain rate of 1×10^{-4} s^{-1}. Three different

levels of plastic strains were detected from the compressive curves. The detailed compressive properties of the uncoated and the two coated Fe-based BMGs are listed in Table 5.1. Here, it is noted that the compressive test results of the three different specimens are highly in line with the empirical "rule of mixtures".

Table 5.1 Summary of the room temperature compressive test results (Young's modulus E, yield stress σ_y, maximum stress σ_m, and plastic strain ε_p) for the uncoated and the Ni coated Fe-based BMGs.

Specimens	E (GPa)	σ_y (MPa)	σ_m (MPa)	ε_p (%)
Uncoated Fe-based BMG	141.0	2925	3325	0.5
29.8 μm Ni coated Fe-based BMG	143.3	2900	3295	2.6
57.7 μm Ni coated Fe-based BMG	146.5	2850	3390	5.0

When comparing the compressive plasticity, the as-cast bare Fe-based BMG only exhibited a limited plasticity of ~ 0.5%, while the 29.8 μm Ni coated Fe-based BMG showed a larger plasticity of about 2.6% and the 57.7 μm Ni coated Fe-based BMG could undergo a remarkable plastic strain of ~ 5.0%. Obviously, the Ni coating exerted a positive effect on the compressive plasticity of the Fe-based BMG without sacrifice of the original ultrahigh strength. Besides, the plasticity was also shown to increase with increasing thickness of the Ni coating.

Fig. 5.6 displays the fracture profiles of the uncoated and Ni coated

$Fe_{75}Mo_5(P_{50}C_{41.67}B_{8.33})_{20}$ BMG after compression. Unlike many other BMG systems such as Zr-based, Cu-based, Ti-based BMGs, one can see from Fig. 5.6(a) that the Fe-based BMG instantly broke into a large number of fragments as soon as crack propagation instability took place. In a conventional silicate glass, a crack often proceeds at a constant velocity, and when the singular component of the stress field at the tip of a crack exceeds a critical value, a single straight crack may become unstable and crack branching occurs, under the premise of linear elasticity. Later on, a fragmentation process prevails under high compressive stress and there are few branch points remaining intact when crack branching is activated [163, 164]. Analogously, a majority of Fe-based BMGs also display an explosive fracture behaviour after compressive loading [24]. It is not uncommon to find a mass of broken branches or fragments which are thought to arise from the destructive micro-branching process. Fig. 5.6(b) and (c) demonstrate that the Ni coated Fe-based BMGs sheared into two large parts which were still wrapped by the coating after failure. This "failure-safe" behaviour allows BMGs to be used in a more reliable fashion and is a good index of safety for engineering structural materials compared with the explosive fracture mode. Fig. 5.7 shows that the shear fractured planes of the uncoated and the two Ni coated Fe-based BMGs were all primarily composed of vein patterns combined with river-like patterns, akin to those on the shear fractured planes of the Zr-based BMGs. Also, on the fractured surfaces of all the tested specimens, many liquid-like droplets could be readily found.

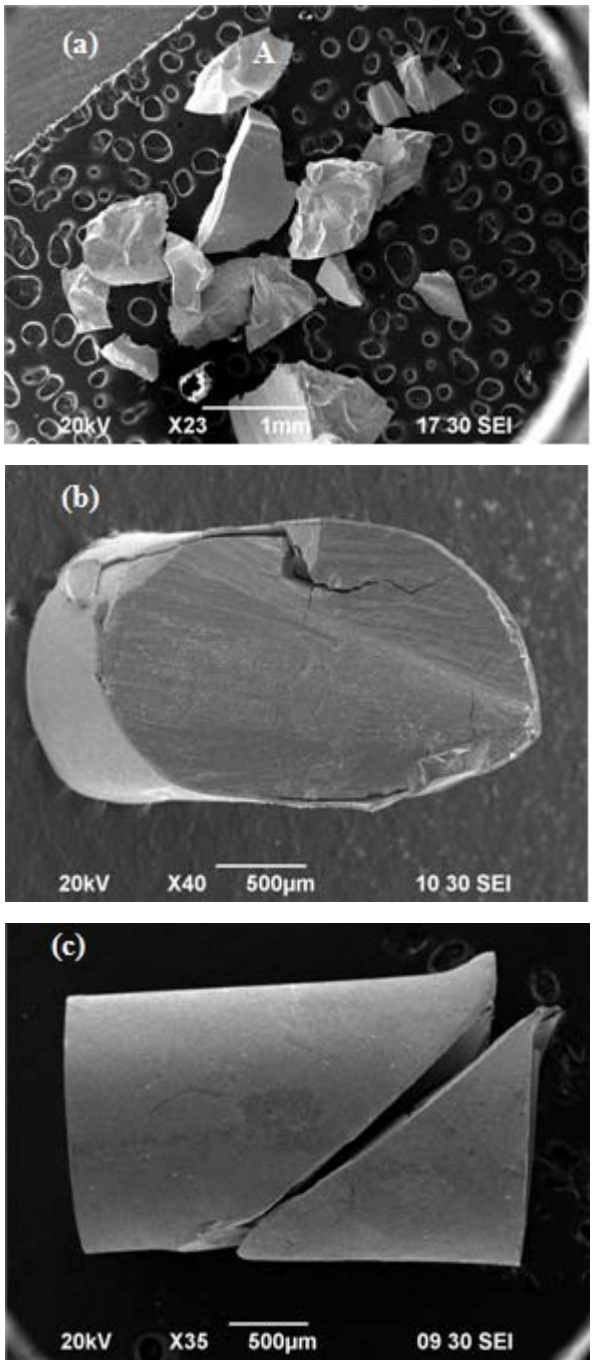

Fig. 5.6 Fracture profile of the (a) uncoated Fe-based BMG; (b) 29.8 μm Ni coated Fe-based BMG; (c) 57.7 μm Ni coated Fe-based BMG.

In addition, it is extremely interesting that if one collects the fracture chips or fragments of the as-cast Fe-based BMGs after fracture, it is not difficult to find that some of the fractured surfaces which emerge as flat mirror surfaces

apparently at the micro-scale virtually hold notable regular periodic corrugated patterns at the nano-scale as shown in Fig. 5.8, which is the enlarged view of the marked area "A" in Fig. 5.6(a). This clearly suggests a microscopically localized plastic deformation associated with a wavy cracking propagation during the fracture process, which behaves in a purely brittle fashion macroscopically [25, 165].

Given that the reasons for the increased plasticity of the Zr-based BMGs induced by Ni coating electroplating have been explained previously in Wang's work [157] by an intensive analysis of the serrated flow behavior of the uncoated and the coated Zr-based BMGs while no work on the mechanical properties of Ni coated Fe-based BMGs has been so far reported. Therefore, in order to recognize the underlying mechanism of the increased plasticity of BMGs by the lateral confining Ni coating in a more deep and universal manner, the notoriously "brittle" Fe-based BMG (i.e., $Fe_{75}Mo_5(P_{50}C_{41.67}B_{8.33})_{20}$ BMG) was taken as the object of the following analysis. Furthermore, rather than only analyzing the serrated flow behavior in the plastic region, there was an attempt to shed light on the role of Ni coating confinement in plasticity enhancement from the perspective of BMG/Ni coating interface interaction observations, which were achieved by two carefully designed interrupt experiments as described below. This can undoubtedly supplement more convincing experimental evidence for interpreting the effect of geometric confinement on plasticity enhancement of

BMGs by electroplated metal coatings.

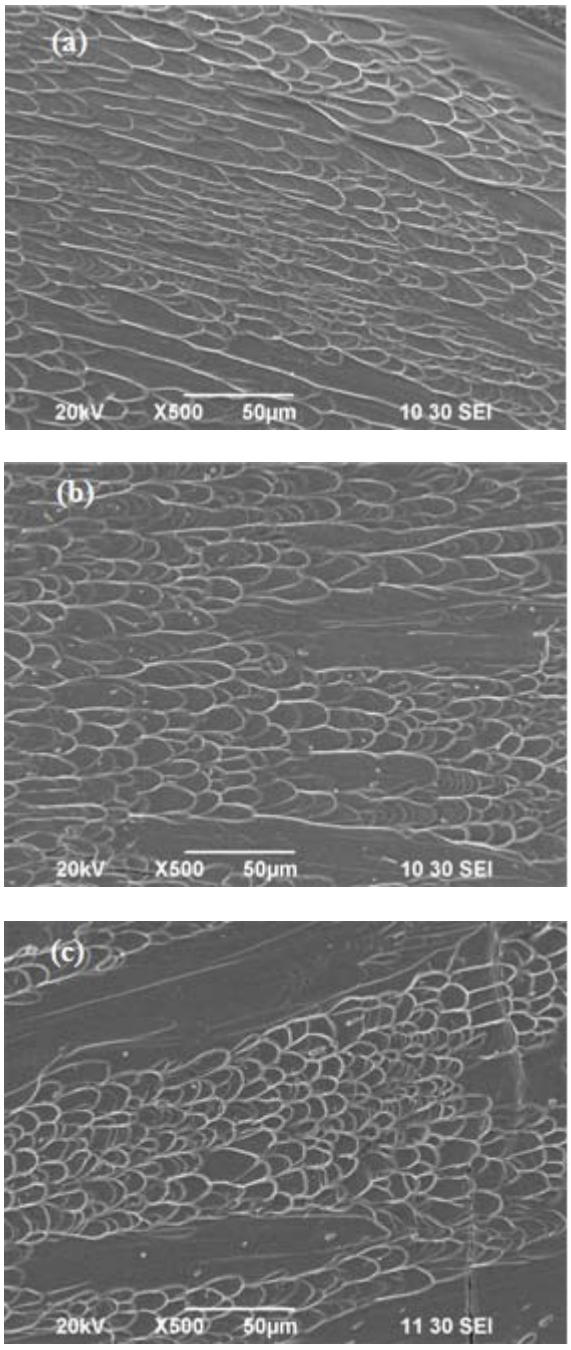

Fig. 5.7 Fracture morphologies of the shear fractured plane of the (a) uncoated Fe-BMG; (b) 29.8 µm Ni coated Fe-based BMG;and (c) 57.7 µm Ni coated Fe-BMG.

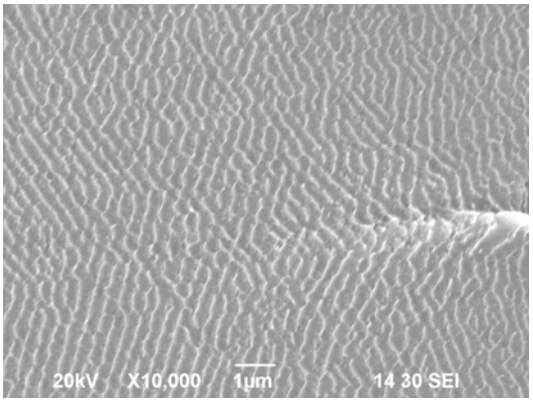

Fig. 5.8 Regular periodic corrugated patterns [enlarged view view of the marked area "A" in Fig. 5.6(a)].

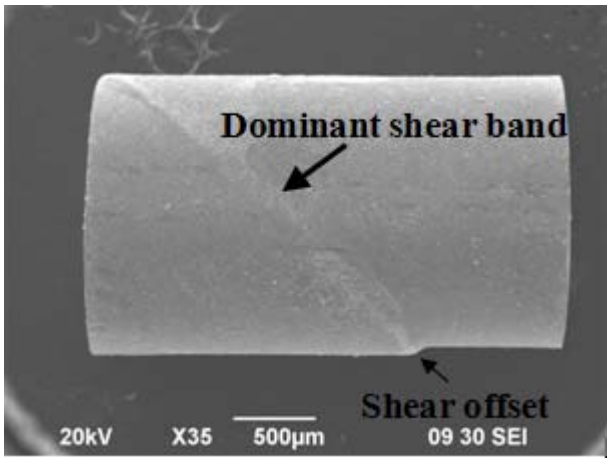

Fig. 5.9 The contour of the 57.7 μm Ni coated $Fe_{75}Mo_5(P_{50}C_{41.67}B_{8.33})_{20}$ BMG that sustained a plastic strain of 4.3% by interrupted experiment.

Fig. 5.9 shows the contour of the 57.7 μm Ni coated $Fe_{75}Mo_5(P_{50}C_{41.67}B_{8.33})_{20}$ BMG, interrupted at a plastic strain of ~ 4.3% after uniaxial compression at a strain rate of 1×10^{-4} s^{-1}. One can unambiguously note a "shear offset" on the side surface of the specimen, reflecting a shear deformation controlled plastic flow. From the compressive stress-strain curve of the 57.7μm Ni coated BMG [Fig. 5.5(c)], a sudden drop in stress was found after achieving a plastic strain of 4%,

after which further deformation was supposed to develop through shear localization exclusively into a narrow shear band called the "dominant shear band" [166]. In this work, it is believed that some of the high plastic strain (~ 5.0%) for this Ni coated Fe-based BMG stemmed from this large "shear offset" along the major shear band before nucleation of the crack. Once this dominant shear band penetrates across the entire specimen, shear instability will occur. Subsequently, cracks that are responsible for the catastrophic failure may nucleate at this dominant shear band. In this regard, it is understandable that previous studies made great efforts to defer the rapid propagation of the major shear band through the introduction of secondary ductile phases into the metallic glass matrix to activate multiple shear bands for accommodating a larger plastic strain [167-169]. In fact, in the present study, the protrusion of the Ni coating on the front of the dominant shear band shown in Fig. 5.9 illustrates that the Ni coating made a great contribution in delaying the shear banding process.

For the purpose of further uncovering the mechanism of the increased plasticity brought by Ni coating electroplating, a standard compressive specimen of the 57.7 μm Ni coated Fe-based BMG was cut with an aspect ratio of 2:1 and the Ni coating was then polished away along the longitudinal direction to expose a smooth surface. This can effectively facilitate visualization of the influence of this Ni coating on the compressive deformation of the Fe-based BMG as well as the Ni coating/BMG interaction in a more vivid and direct manner. At around 3% plastic strain, the compression test was interrupted and the surface of the

polished cross-section was examined by SEM, as shown in Fig. 5.10. Evidently, two sets of parallel shear bands appear on the surface of the sample in two directions, as shown in Fig. 5.10(a), one set has an angle of ~ 45° to the compressive direction, called primary (or major) shear bands, and another perpendicular to the loading direction, named secondary shear bands. The branching of the primary shear bands can be one origin responsible for the multiple nucleation of the shear bands. Another important reason for the activation of multiple shear bands is thought to be the stress concentration at the interface between the Ni coating and the Fe-based BMG. This stress concentration promoted the preferential nucleation of multiple shear bands at the BMG/Ni interface. The stress concentration might come from the following two aspects. For one thing, it is well known that the process of Ni coating electroplating brings about residual compressive stress at the interface and this stress is empirically in direct proportion to the coating thickness and keeps nearly constant after the coating thickness exceeds 50 μm [170]. For another, during the loading period, both the BMG and the coating expand towards the radial direction until failure. Since Poisson's ratio of the brittle Fe-based BMGs is lower than the critical brittle/ductile transition value of 0.32 [18, 108, 110, 171, 172] and much lower than that of the Ni coating electroplated from Watts electrolyte (0.36) [173], the Ni coating expanded more than the BMG along the radial direction upon uniaxial compression. This excessive lateral expansion in the Ni coating caused by the mismatch in Poisson's ratio between the Fe-based BMG

(v_B) and the Ni coating (v_c) resulted in a relaxation of lateral confining stress σ_c imposed on the BMG, as predicted by equation (2.8). When the loading stress reached the yield strength of the Ni coating, the exerted compressive stress by the Ni coating achieved a maximum value $\sigma_c^{\max}$ approximated by [122]:

$$\sigma_c^{\max} = \sigma_y \ln \frac{b}{a} \tag{5.2}$$

where σ_y is the yield strength of the Ni coating; a and b are the diameters of the uncoated Fe-based BMG and the coated Fe-based BMG, respectively. This relaxation in lateral confining pressure did not disappear or release until

$$(\upsilon_c - \upsilon_B)\varepsilon \geq \frac{\sigma_y}{E_c} \tag{5.3}$$

was reached [28], where ε represents for the axial strain for both the Fe-based BMG and the Ni coating; E_c refers to the Young's modulus of the Ni coating electroplated from the Watts solution (207 GPa) [173]. If one approximates v_B = 0.30 ~ 0.31, v_c = 0.36, E_c = 207 GPa, σ_y = 1000 MPa, and substitute these values into above equation, then it can be deduced that ε = 8% ~ 9.7%. This means that the outer Ni coating can maintain a high confining pressure on the Fe-based BMG before a possible maximum plastic strain of 8.0% ~ 9.7% is reached. Thus, it is desirable that the confining coating can not only exert a high confining pressure, but maintain the high confining pressure on the BMGs so as to achieve a reliable confinement effect.

The compressive stress at the interface coming either from the electroplating

process or Poisson's ratio mismatch is beneficial for activating the multiple shear bands nucleation and thus improving the plasticity, as proven previously [12]. Moreover, predicting from equations (2.8) and (5.2), it should be noticeable that during compressive loading, the thicker the Ni coating, the higher the confining stress, which coincides with the different plastic strains for two different thick Ni coated samples. This dependence of plasticity improvement on the level of confining stress was well compatible with that reported by Ashby *et al* [174], who found that confined heterogeneous brittle crystalline solids, such as ice, rocks and ceramics, display three categories of deformation behavior depending on the confining stress level under uniaxial compressive loading. To be specific, uniaxial compression of the brittle solids under no or a low confining stress often lead to a severe brittle failure of explosive slab fragments which run parallel to the maximum compressive stress. Upon a medium lateral confining pressure, a macroscopic shear failure prevails in the uniaxial compressive deformation of brittle solids. However, if the confining pressure reaches a certain high level, the brittle solids can even deform in a pseudo-ductile or ductile way, and this brittle-to-ductile transition was also observed in ceramics under high confining stresses by Heard and Cline in 1980 [175].

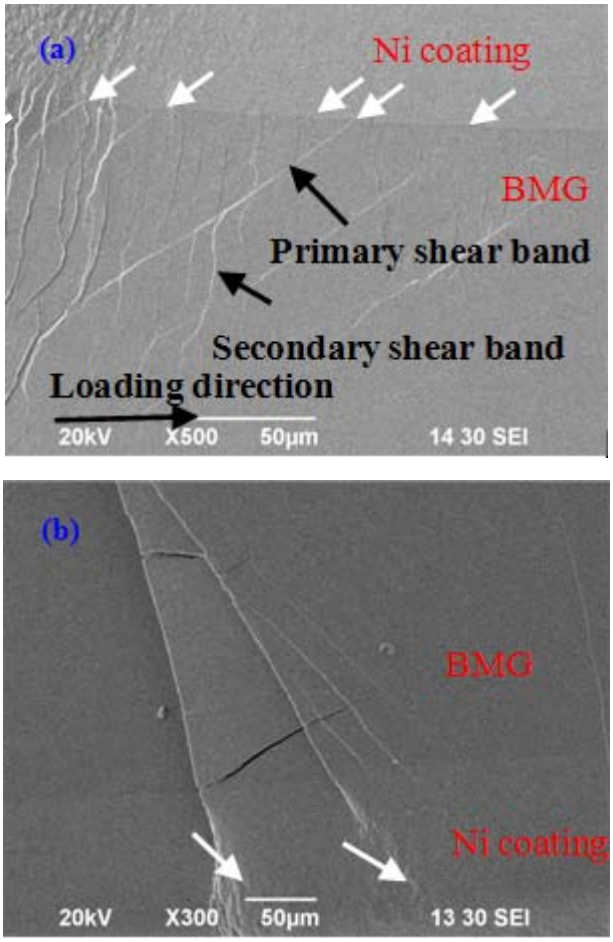

Fig. 5.10 (a) Multiple shear bands initiated on the polished surface of the Fe-based BMG; (b) Arrest of shear band propagation by Ni coating.

In fact, Fig. 5.10 also clearly illustrates that during the shear band propagation process, the Ni coating can behave as barrier to hinder the propagation of the shear bands by means of self-deformation (shown by the white arrows) to dissipate the elastic energy stored within the BMG. Once the individual shear band propagation is arrested, shear band bifurcation may follow, seeding the initiation of multiple shear bands to accommodate more shear strain in many shear planes. Hence, this absorption of elastic deformation energy by Ni coating confinement makes a considerable contribution to the plasticity enhancement of

the BMGs and the stabilization of the shear banding behavior, in accordance with the previous prediction that searching for avenues to absorb the elastic deformation energy should be effective in the toughening of BMGs.

5.3 Toughening BMGs by a Cu/Ni bilayered coating confinement

To study the effect of a bilayered Cu/Ni coating, in comparison with a mono-layered Ni coating or mono-layered Cu coating, on the mechanical behavior of BMGs. $Zr_{57}Al_{10}Ni_8Cu_{20}Ti_5$ BMG was taken as the research target and was electroplated with a layer of about 80 μm Cu/Ni, pure Cu coating, pure Ni coating [as the 76.6 μm Ni coated Zr-based BMG described in Fig. 5.1(b)], respectively. All the cross-sections of the three different coated Zr-based BMGs are shown in Fig. 5.11. The thicknesses of all the coatings were maintained at around 80 μm ± 5 μm in order to minimize the effect on the compressive behavior. For the 80 μm mono-layered Cu coated BMG, electroplating was done for 160 min whereas it was conducted for 3 hrs for the 76.6 μm mono-layered Ni coated BMG as illustrated above. In the case of the Cu/Ni bilayered coating, Cu and Ni plating were carried out for 1 hr and 6 hrs, respectively, using the two-step dual bath electroplating technique.

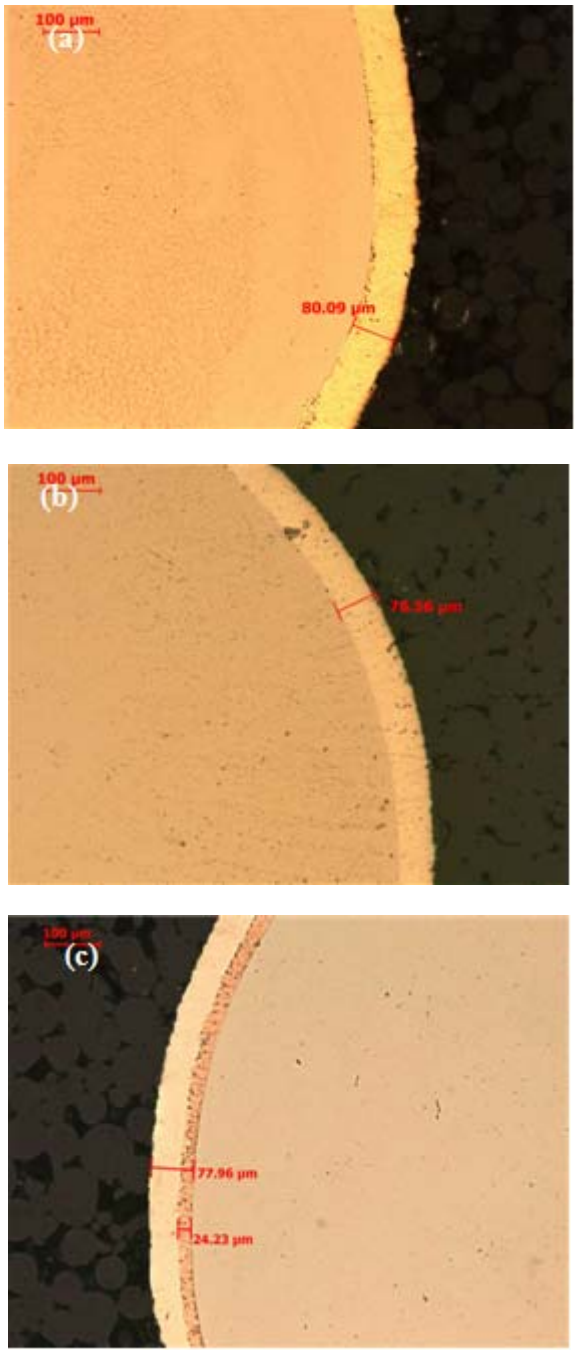

Fig. 5.11 Cross-sections of the Zr-based BMGs with different coatings: a) 80.1 µm Cu coating; b) 76.6 µm Ni coating; c) 77.9 µm Cu/Ni coatings (24.2 µm Cu coating, plus 53.7 µm Ni coating)

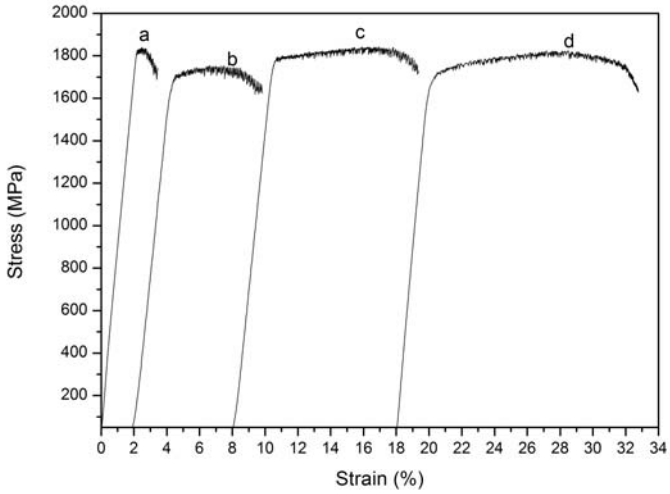

Fig. 5.12 Compressive stress-strain curves of the different samples: a) as-cast Zr-based BMG; b) Cu coated Zr-based BMG; c) Ni coated Zr-based BMG; d) Cu/Ni coated Zr-based BMG.

The engineering stress-strain curves of the as-cast Zr-based BMG and various coated Zr-based BMG samples are plotted in Fig. 5.12. The yield strength and compressive plasticity derived from the stress-strain curves are summarized in Table 5.2. As stated previously, the as-cast specimen yielded at 1807 MPa with a limited plastic strain of 1.3%. The pure Cu coated BMG yielded at a substantially lower stress of only 1535 MPa, followed by a plastic strain of 5.6%. By contrast, the pure Ni coated specimen and the bilayered Cu/Ni coated samples yielded at 1729 MPa and 1610 MPa, respectively, and their respective plastic strains were 8.9% and 12.9 %. Again, the measured yield strengths of the coated BMGs are roughly consistent with the calculated theoretical values according to the "rule of mixtures".

Table 5.2 Summary of the yields strength and plasticity of as-cast, Cu coated, Ni coated and Cu/Ni coated Zr-based BMGs.

Specimens	σ_y (MPa)	ε_p (%)
Uncoated Zr-based BMG	1807	1.3
Cu coated Zr-based BMG	1535	5.6
Ni coated Zr-based BMG	1729	8.9
Cu/Ni coated Zr-based BMG	1610	12.9

If one carefully observes all the compressive stress-strain curves for different specimens, it is found that the amount of serrations monotonously increases with the increase of plasticity, reflecting the growth of the density of shear bands accompanied by the plasticity enhancement. Experimental observations of the shear band traces on the different deformed BMGs after compression further verify this assumption, as displayed in Fig. 5.13. In Fig. 5.13(a), few shear bands can be seen on the as-cast specimen, which suggests that the main shear band, after activation, propagated rapidly out of the surface of the BMG. On the Cu coated BMG, a couple of sparse parallel shear bands can be detected [Fig. 5.13(b)]. In contrast, a large number of shear bands appear on the pure Ni coated BMG and the Cu/Ni coated BMG. In the pure Ni coated sample shown in Fig. 5.13(c), a large number of shear bands which can be categorized into two parallel groups perpendicular to each other are captured. Fig. 5.13(d) discloses that more dense shear bands are homogeneously distributed on the Cu/Ni coated sample.

These shear bands, compared with those on the pure Ni coated sample, seem to be somewhat randomly arranged in orientation. Furthermore, a colossal number of tenuous branched secondary and tertiary shear bands are found to be eradiated from and intersect with the primary shear bands all over the side surface, which suggests a significant homogeneous plastic deformation instead of a highly localized shear deformation. This concurrent emission of multiple shear bands dissipates much more loading energy, accounting for the numerous minor serrations and the high plastic deformation strain, just as revealed in the compressive curve.

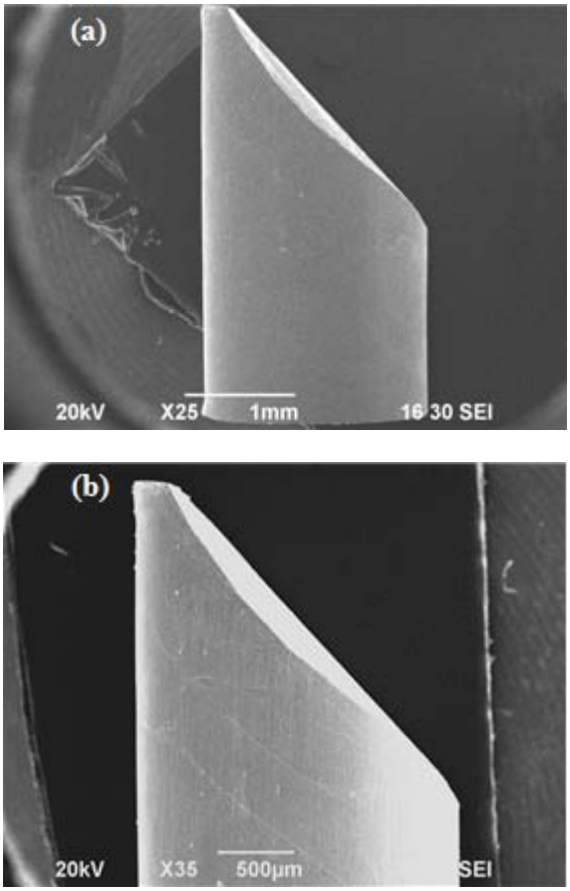

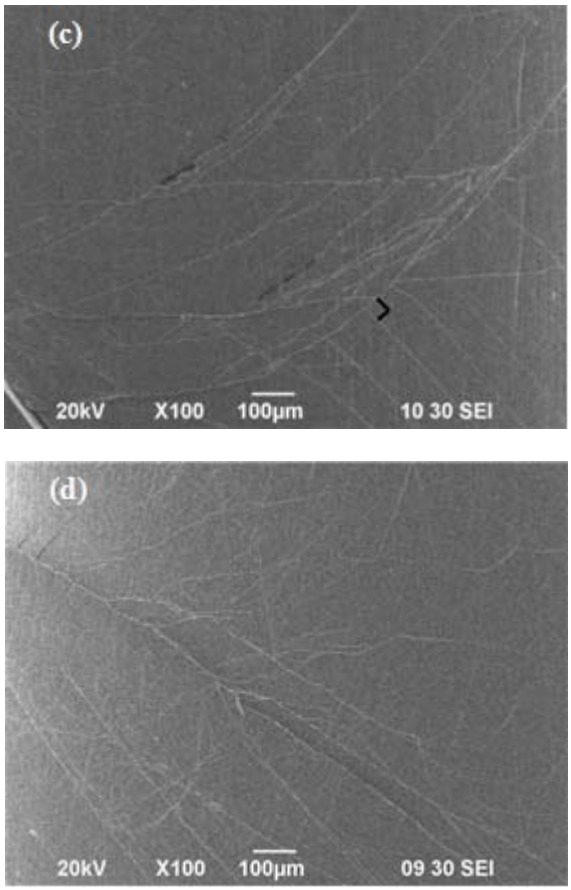

Fig. 5.13 Fracture morphologies of the different specimens after compression: (a) as-cast Zr-based BMGs; b) Cu coated Zr-based BMG; c) Ni coated Zr-based BMG and d) Cu/Ni coated Zr-based BMG.

In order to elucidate the effect of different coatings, the mechanisms for the enhancement of plasticity are discussed in terms of residual stress, confining stress and the Cu/Ni interface strength. Usually the Cu coating obtained from the acid sulfate baths is stress-free or contains negligible residual stress [26], while the residual compressive stress involved in the Ni plating process from the hard Watts baths can reach up to 280 ~ 340 MPa [29]. On the other hand, the radial confining stress exerted on the BMG σ_c is linearly proportional to the yield strength of the coating σ_y, as indicated in equations (2.8) and (5.2). Considering

that the strength of the Ni coating is nearly 6 ~7 times higher than that of the Cu coating, the loading induced confining stress by the Cu coating is far lower than that by the Ni coating. Hence, when comparing the plasticity of the Cu coated BMG and the Ni coated BMG, although the Ni coating is much more brittle than the Cu coating, (i.e., based on the "crack buffer zone" model, the ~ 20 μm thick Ni coating in contact with the BMG may not be as effective as Cu coating) the much higher overall strength of the Ni coating and the residual stress brought by the Ni plating process led to an overwhelming confining stress superimposed on the BMG during loading, which well compensated the brittleness of Ni coating and promoted the multiplication of shear bands. Consequently, the Ni coated sample carried a larger plasticity than the Cu coated sample.

Afer the Cu/Ni coated BMG is concerned, the 53.7 μm Ni layer plating can produce nearly an equivalent residual compressive stress as pure 76.6 μm Ni plating since this residual stress in the Ni plating is highly dependent on the deposition rate, and it remains constant at a thickness in excess of 50 μm [170]. Apart from this Ni plating induced residual stress, there are other types of stresses that can give rise to the overall intrinsic compressive stress in the Cu/Ni bilayer system: the modulus mismatch (named the Koehler barrier) and the gamma surface mismatch (chemical interaction) may introduce localized compressive stresses at the Cu/Ni interface; the lattice parameter mismatch may generate oscillating coherency stresses and misfit locations at or near the Cu/Ni

interface [176]. These stresses effectively enhance the overall residual stress in the Cu/Ni deposit.

In terms of the strength of the Cu/Ni bilayered coating, which directly determines the level of the lateral confining stress, the theoretical yield strength of the Cu/Ni bilayer is calculated to be about 730 MPa according to "rule of mixtures", being just a little lower than the strength of the pure Ni coating. Yet, the modulus mismatch (Koehler barrier), the slip plane mismatch, and the lattice parameter mismatch between the Cu and the Ni layer might remarkably strengthen the Cu/Ni coating [176, 177]. The Koehler barrier is an effective obstacle to the dislocation movements in the Cu/Ni system, and the slip-plane mismatch requires mobile screw dislocations to cross-slip and forces other dislocations to leave a different dislocation at the interface; while the lattice parameter mismatch may generate oscillating coherency stresses and misfit locations at or near the Cu/Ni interface, which can not only enhance the Koehler barrier but also prevent or retard the dislocation glides released from the inner Cu layer. Due to the presence of these barriers, the failure strength of the Cu/Ni is effectively enhanced. If the stress at which the interface obstacle of this bilayered coating system can be overcome is defined as the "blocking strength", then this blocking strength has been roughly estimated through atomic simulation to be as high as ~1.24 GPa [176]. Such a substantial high blocking strength is inevitably beneficial for the creation of a high external confining stress. Furthermore, it is

meanwhile notable that the inner Cu layer in the Cu/Ni bilayer, being superiorly ductile in comparison with the brittle Ni coating, and can be regarded as an effective shear strain and elastic deformation energy storage area that adequately absorbs the shear banding energy and crack propagation energy by means of its strong deformability through dislocations operations without premature formation of micro-cracks, which may otherwise take place if localized in the brittle Ni coating. Taking these into account, the confining effect generated in the case of the Cu/Ni coated BMG outweighs that in the mono-layered Ni coated specimen. This strong confining effect aids the restriction of the shear band movements or micro-crack propagation and rather promotes the initiation of multiple shear bands, thereby improving the macroscopic plastic deformation.

5.4 Summary

Through the experimental investigations, the geometric confinement by metal coating electroplating is found to be effective in enhancing the plasticity of not only Zr-based BMGs but also the ultrahigh strength Fe-based BMGs. The geometric confinement effectiveness by the electroplated metal coating is found to increase with increasing coating thickness.

By electroplating a Cu/Ni bilayered coating onto the side surface of the $Zr_{57}Al_{10}Ni_8Cu_{20}Ti_5$ BMG, it was found that the role of geometric confinement in plasticity enhancement of BMGs by this bilayered coating outweighs that by an

equivalent thick mono-layered Cu or mono-layered Ni coating. The inner soft Cu layer behaves as a good "crack buffer zone" to effectively absorb the elastic deformation energy released by BMGs during loading; while the outer layer of the strong Ni coating plays a significant role in exerting a high confining stress. Additionally, the high blocking strength of the strong Cu/Ni interface arising from the modulus mismatch, the slip plane mismatch, and the lattice parameter mismatch between the Cu and Ni layer is also believed to contribute to the geometric confinement effectiveness.

Chapter 6 Combined effects of loading boundary friction reduction and geometric confinement

6.1 Influence of loading boundary friction on compression behavior

Generally, there are two limitations in the validity of compression testing in assessing the plastic deformation behavior of materials: friction and buckling. The elastic mismatch between the loading platens and the compression sample often results in frictional boundary restraints at the loading boundaries (interfaces between the platens and the sample) [142]. Buckling is prone to take place when the specimen is too long and slender, especially when the aspect ratio exceeds 3:1. Buckling can be avoided or substantially eliminated by means of decreasing the aspect ratio to less than 3:1. Paradoxically, the reduction of aspect ratio invokes the increase of friction at the loading boundary.

The frictional constraints at the loading boundaries strongly influence the compressive behavior of disordered and brittle materials. For instance, it has been widely acknowledged that concrete materials usually display different yield strength and plastic deformation with alteration of the friction conditions [178]. Due to the presence of friction, a cone-shaped region where non-deforming material, called "dead material" can form at each loading boundary as depicted in Fig. 6.1, and a higher load is required to overcome the friction and to activate

plastic deformation. As a result, the test specimen appears to be barrel shaped, and the frictional constraints on the two ends of the sample are likely to produce shear stresses at the interfaces between the loading platens and the specimen. These shear stresses act inwards and develop a "clamping" effect that suppresses as the lateral spreading of the materials near the ends, which causes inhomogeneous stresses or strains within the sample [142, 179].

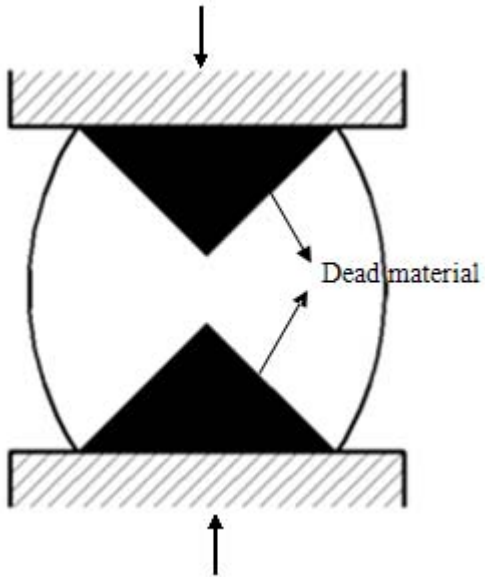

Fig. 6.1 Schematic diagram of "dead material" at each loading boundary.

6.2 Enhanced plasticity of BMGs by encapsulating BMGs into Cu coatings

Notwithstanding the influence of frictional restraint optimization by the insertion of Cu foils at the loading boundaries on the mechanical behavior of BMGs has been reported [13], whether Cu coating electroplating on each end of the BMGs can play a positive role in lessening friction at the loading boundary is still unknown. In order to clarify this, about 85 μm Cu coatings were electroplated on

the two ends of the $Zr_{57}Al_{10}Ni_8Cu_{20}Ti_5$ BMG, and the mechanical properties of this two end Cu coated sample were compared with the uncoated as well as the completely Cu-coating encapsulated $Zr_{57}Al_{10}Ni_8Cu_{20}Ti_5$ BMG. All the compression samples with an aspect ratio of 2:1 are displayed in Fig. 6.2(a). Each Cu coated sample was electroplated for 3 hrs using a stable current density of 0.2 mA/mm^2 ± 0.01 mA/mm^2 at room temperature.

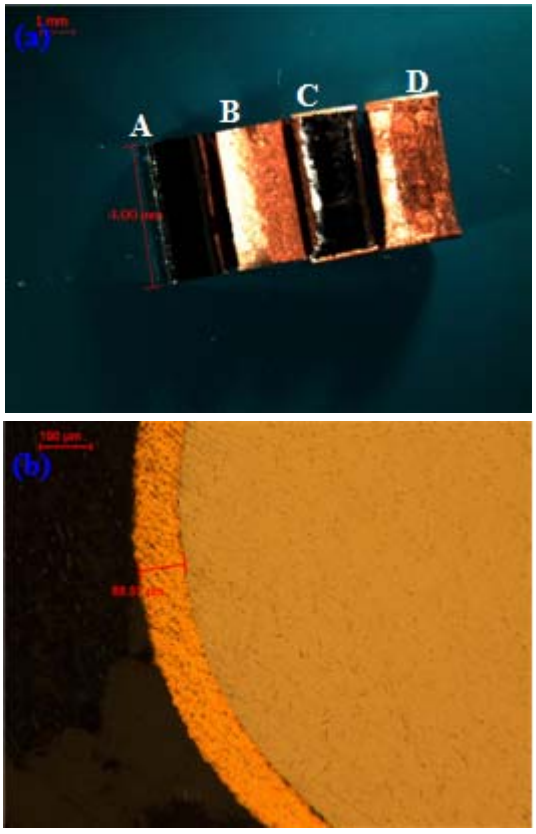

Fig. 6.2 (a) A view of four different compression BMG samples: uncoated Zr-based BMG (A), laterally Cu coated Zr-based BMG (B), two ends Cu coated Zr-based BMG (C) and completely Cu-coating encapsulated Zr-based BMG (D); (b) Cross-section of the Cu coating on the side surface of the Zr-based BMG samples.

From Fig. 6.2(a), one can find that the two ends of each sample for compression were ground parallel and perpendicular to the lateral surface. Fig. 6.2(b) reveals that the thickness of the Cu coating obtained on the side surface is approximately 85 μm after 3 hrs of electroplating and the thicknesses of the coatings on the two ends of the specimen were all measured to be 85 μm ± 5 μm by a precision micrometer.

Fig. 6.3 displays the true compressive stress-strain curves of all the tested specimens. The mechanical properties are summarized in Table 6.1. The laterally Cu coated Zr-based BMG had a slightly higher Young's modulus but lower yield strength than the uncoated BMG, which can be understood in terms of the "rule of mixtures" as discussed previously. Young's modulus and yield strength of the two end coated Zr-based BMGs were found to be much lower than in the uncoated and laterally coated specimens. In fact, the two end coated samples can be regarded as a sandwich structured material. However, upon uniaxial loading, the equal strain hypothesis does not apply to this sandwich on the grounds that the Cu coatings on the two ends have a considerably lower yield strength than for the Zr-based BMG. As long as the external loading stress approaches the yield strength of the Cu coating, i.e., 120 ~ 150 MPa, the Cu coatings on the two ends tend to deform in advance of the Zr-based BMG [180]. Fig. 6.4 magnifies the true stress-strain curves within the compressive stress range of 50 MPa ~ 400 MPa for the uncoated, laterally coated and two end coated specimens,

respectively. Obviously, the uncoated and laterally coated Zr-based BMGs experienced a pure elastic deformation in this loading range. By contrast, the two end coated BMGs had sustained some irreversible plastic strain during this stage because the Cu coatings on the two ends had undertaken some plastic strains and shown their superior deformability, accompanied by the "work-hardening" effect in this loading regime. The elastic mismatch between the Zr-based BMG and the Cu coating lends convincing support for the sharp decrease of Young's modulus measured by the MTS system, which automatically neglects the negligible deviation from linear elasticity until yielding. On the basis of these discussions about the mechanical properties of the laterally coated and the two end coated BMGs, it is reasonable to obtain the lowest Young's modulus and yield strength in the case of the completely encapsulated specimen, if both the sandwich and laminate models are taken into consideration. The most impressive results in Table 6.1 are the different plasticities for the four different samples. The coated BMGs all carried a larger plasticity than the uncoated one, especially for the completely wrapped sample, which undertook a plastic strain of approximately 20% before failure. This degree of plasticity improvement is even more notable than many of the widely utilized secondary nanocrystalline phase reinforcement methods for numerous BMG composites [181, 182].

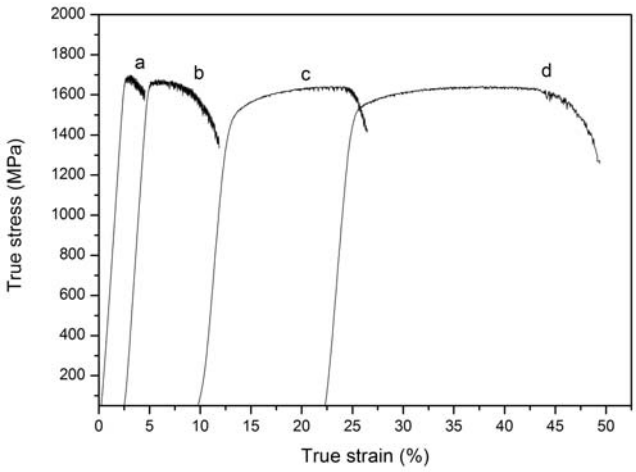

Fig. 6.3 The true compressive stress-strain curves of the (a) uncoated Zr-based BMG; (b) laterally Cu coated Zr-based BMG; (c) two ends Cu coated Zr-based BMG; (d) completely Cu-coating encapsulated Zr-based BMG.

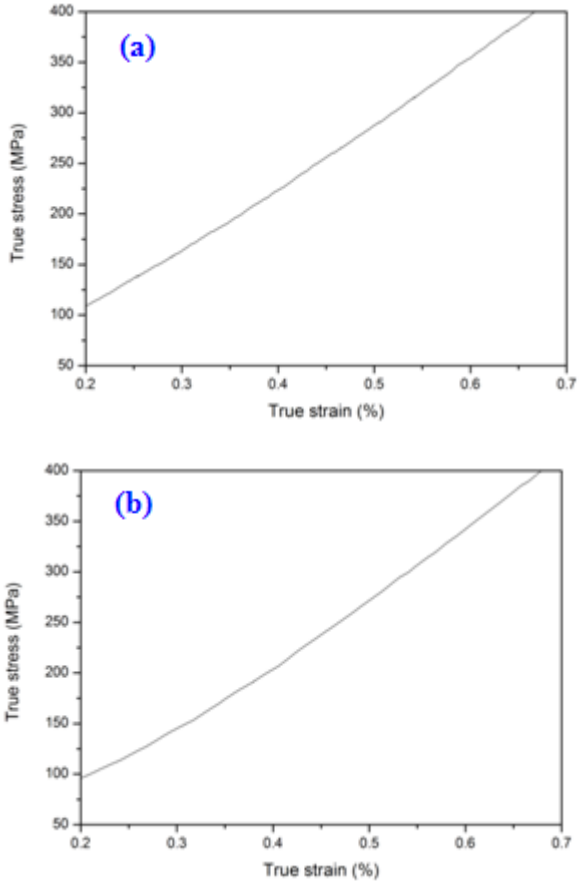

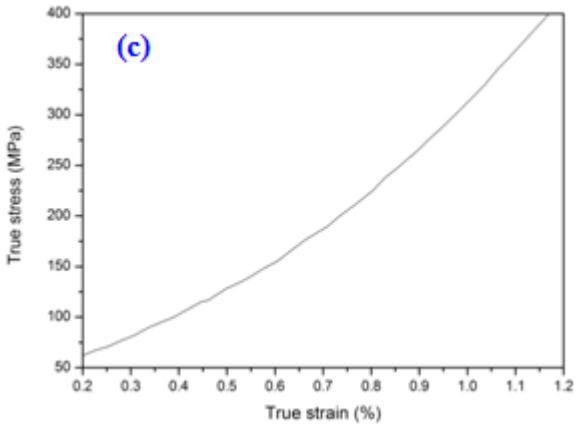

Fig. 6.4 Partial elastic regime upon loading for the different samples: (a) uncoated Zr-based BMG; (b) laterally wrapped Zr-based BMG and (c) two ends coated Zr-based BMG.

Table 6.1 Summary of the room temperature compressive test results derived from the true compressive stress-strain curves (Young's modulus E, yield stress σ_y, maximum stress σ_m, and plastic strain ε_p) for all the tested BMGs.

Specimens	E (GPa)	σ_y (MPa)	σ_m (MPa)	ε_p (%)
Uncoated BMG	72.1	1614	1685	2
Laterally coated BMG	75.0	1562	1674	6.5
Two ends coated BMG	63.7	1290	1647	13
Completely encapsulated BMG	64.5	1310	1641	20

Carefully observing the compressive curves of the different specimens in Fig. 6.3, one can note that the plastic flow regions of the four specimens are significantly different from the several compressive curves shown in previous Sections, in particular for the two end coated and the completely encapsulated samples, where "work-hardening" invoked stress increase was surprisingly discovered. It is therefore significant to scrutinize the plastic flow regimes of the different specimens in depth. The plastic flow regimes in the compressive stress-strain curves all exhibited flow serrations after yielding. The serrations for different compressive specimens are magnified in Fig. 6.5. It has been extensively agreed that one serration event involves a process of elastic energy accumulation, and a process of elastic energy release. The stress drop in a serration event can be considered as a result of the emission/propagation of shear bands [183]; while the stress increase is believed to stem from the blunting of shear bands or micro-cracks. In this sense, if one serration is regarded as a shear band emission, the shear band density or the number of shear bands on the deformed specimen can be roughly estimated according to the number of serrations. For that matter, since the plastic strain of BMGs is usually accommodated in the shear bands through shear localization, it is reasonable, based on the amount of discernible serrations, to deduce the plasticity of BMGs. In practice, the serrations in the compressive curves of different specimens shown in Fig. 6.5 agree well with the different levels of measured plasticity. From all the curves in Fig. 6.5, it is also obviously visible that in the different stages of plastic deformation, different

serrated fluctuations appear. To be specific, the stress fluctuations during the onset of plastic strain (just after yielding) are quite small while moderate stress fluctuation takes place in the steady plastic flow regime, followed by unstable deformation before failure, where stress fluctuations become increasingly pronounced. Furthermore, close scrutiny of the serrations of different specimens indicates that compared with the uncoated specimen, more tiny and moderately fluctuated serrations are present in the stress-strain curves of the laterally coated sample. This phenomenon is far more notable in the other two specimens, i.e., the two end coated and the completely Cu-coating encapsulated specimens. Quantitatively, if the shear band density is evaluated according to the total number of shear band events per specimen, the shear band density of the uncoated BMG is calculated to be about 30, while the value for the laterally coated BMG is measured to be approximately 85, which is nearly three times that for the uncoated BMG. In the same way, the shear band density of the two end coated specimens and the completely encapsulated specimen can be derived from Fig. 6.5 to be 134 and 193, respectively. The different degrees of shear band density agree well with the different levels of plasticity, suggesting again that the plasticity of BMGs during compressive deformation can be roughly estimated by the shear band amount. Furthermore, from Fig. 6.5, it can also be inferred that the large plasticity of the coated BMGs is a consequence of the large number of tiny and moderate serrations during the plastic regime (especially the platform stage of the plastic deformation). Except for these, a "work-hardening" effect in

the two end coated and the completely wrapped specimens (marked by arrows) was surprisingly found, which is strongly conducive to engineering safety. To study this effect, microhardness (Vickers hardness) tests were further performed and the results are presented later.

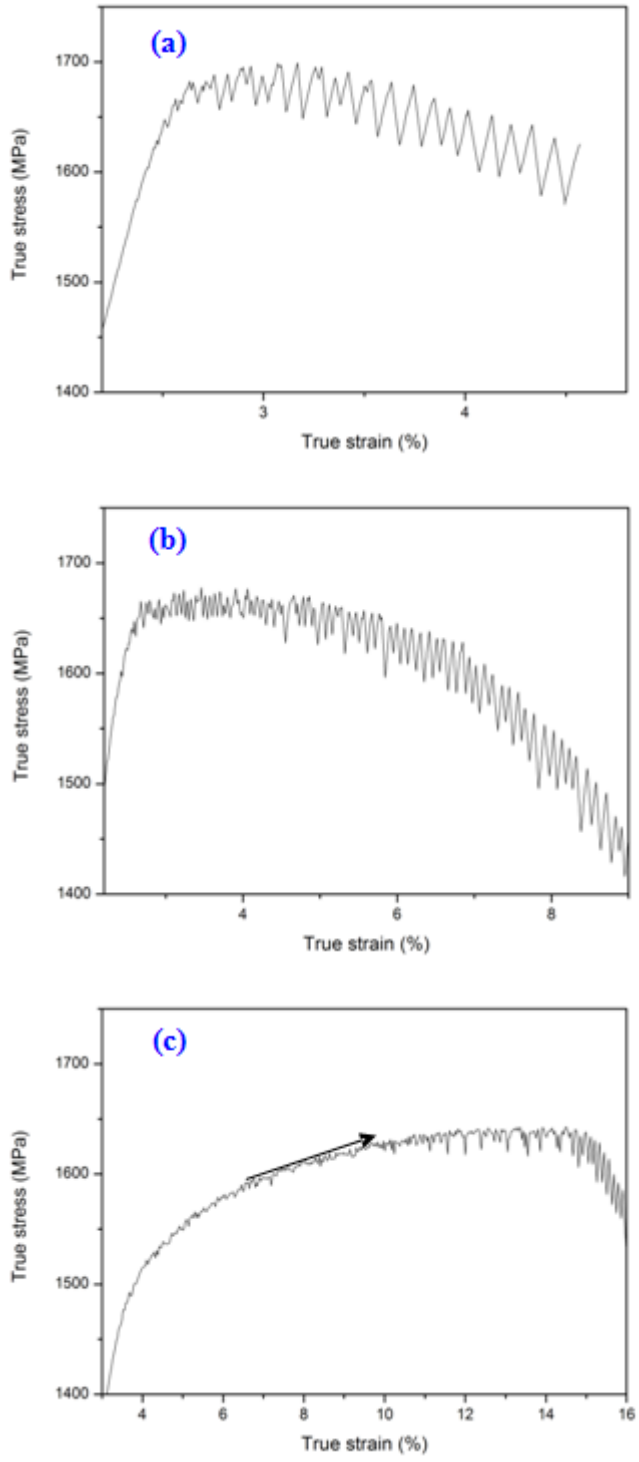

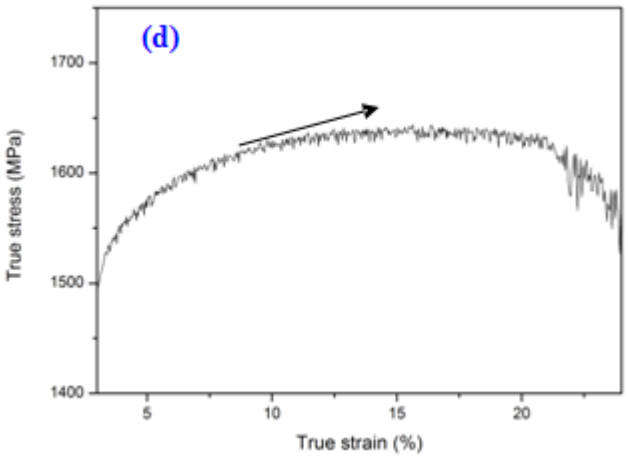

Fig. 6.5 Enlarged serrations of different samples during plastic regime: (a) uncoated Zr-based BMG; (b) laterally coated Zr-based BMG; (c) two ends coated BMG and (d) completely Cu-coating encapsulated Zr-based BMG.

Fig. 6.6 shows the side views of all the tested specimens after fracture. Different densities of shear bands on the different specimens are displayed. Compatible with the limited plasticity, the side surface morphology of the uncoated specimen exhibits barely visible shear bands. On the laterally coated specimen, somewhat denser paralleled shear bands can be found near the dominant shear fractured plane. As for the two end coated and the completely encapsulated samples, shear bands are found uniformly distributed on the entire specimens and they can be categorised into several distinct networks: one set of semicircular shear bands adjacent to the edge in contact with the Cu coating at two ends, another two sets of shear bands parallel and perpendicular to the major shear plane and the bridging parallelled shear bands in the horizontal direction. The different densities of shear bands in Fig. 6.6 further verify that a larger ductility is associated with a higher shear band density. Furthermore, multiple "shear offsets"

or "slip steps" are unambiguously observed in Fig. 6.6(c) and (d), marked by the white arrows. These multiple "shear offsets" or "slip steps" actually recorded large plastic strains accommodated in different shear planes. Normally, BMGs deform or even slip along a major shear plane via shear localization. In this study, the interaction between the multiple shear band networks helps to defer the rapid shear banding along the single major shear plane and forces the plastic strain to be dispersed into different shear planes instead, thus stabilizing the shear banding process and improving the macroscopic plasticity.

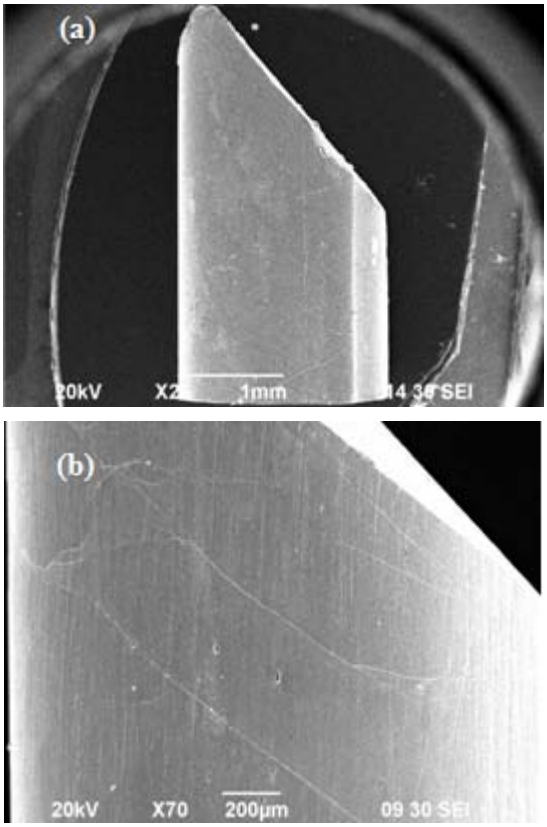

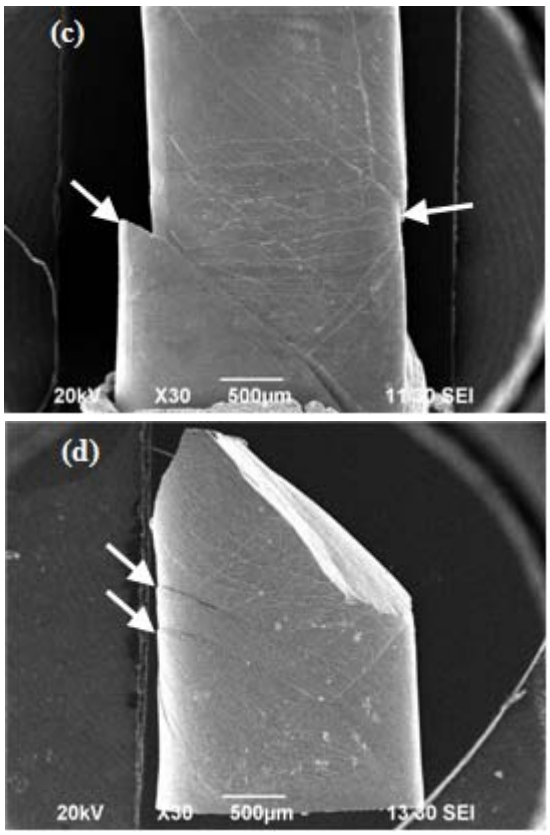

Fig. 6.6 The side surface of the fractured specimens after compression: (a) uncoated Zr-based BMG; (b) laterally coated Zr-based BMG; (c) two ends coated Zr-based BMG and (d) completely encapsulated Zr-based BMG.

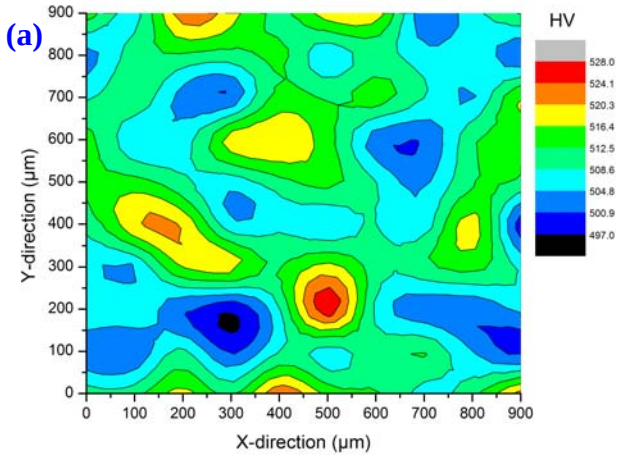

(b)

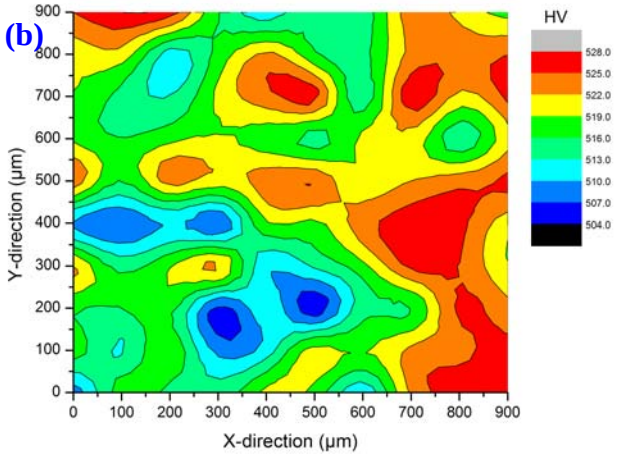
HV
528.0
525.0
522.0
519.0
516.0
513.0
510.0
507.0
504.0
Y-direction (μm)
X-direction (μm)
0
100
200
300
400
500
600
700
800
900

(c)

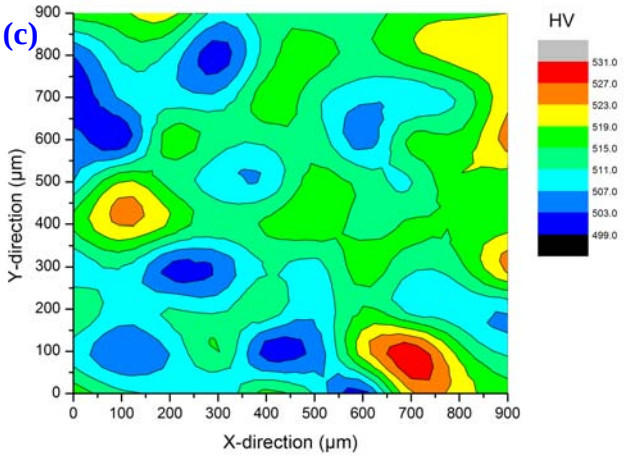
HV
531.0
527.0
523.0
519.0
515.0
511.0
507.0
503.0
499.0
Y-direction (μm)
X-direction (μm)
0
100
200
300
400
500
600
700
800
900

(d)

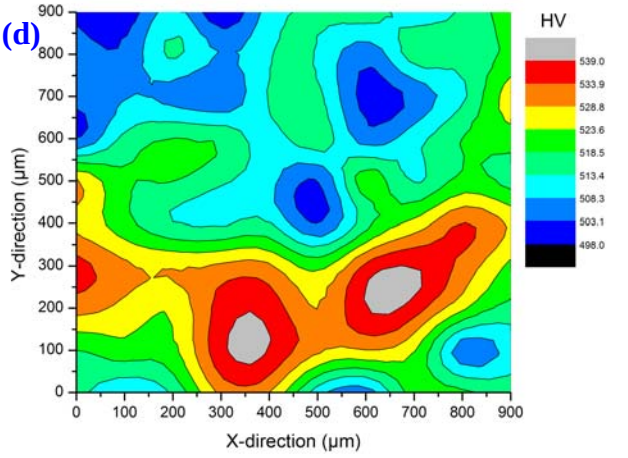
HV
539.0
533.9
528.8
523.6
518.5
513.4
508.3
503.1
498.0
Y-direction (μm)
X-direction (μm)
0
100
200
300
400
500
600
700
800
900

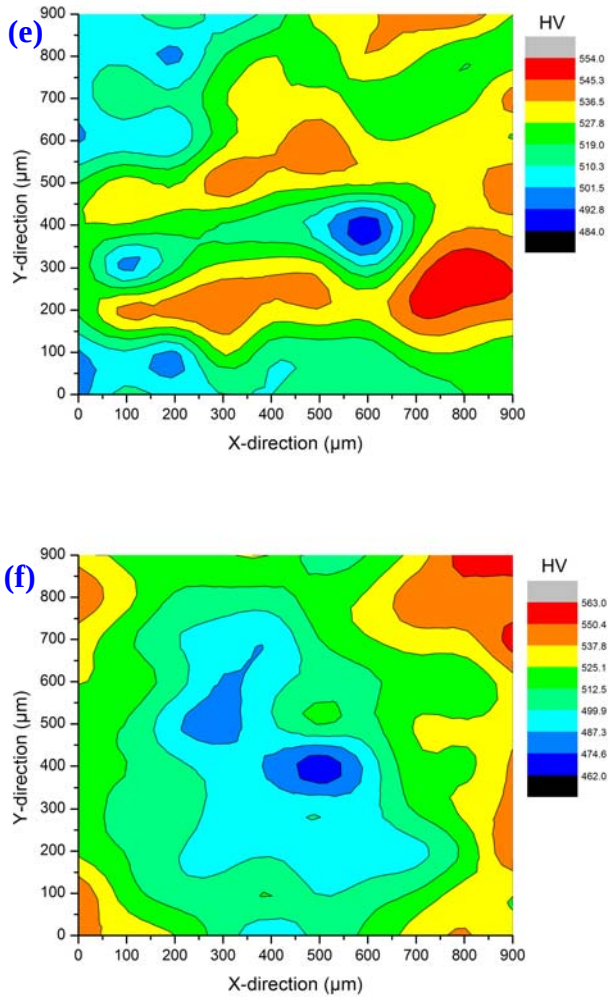

Fig. 6.7 The microhardness contour maps of different specimens, (a) uncoated BMG (as-cast); (b) uncoated BMG after fracture; (c) electroplating pre-treated BMG prior to compression; (d) laterally coated BMG after fracture; (e) two ends coated BMG after fracture; (f) completely encapsulated BMG after fracture.

The Vickers microhardness maps of different states of BMGs are demonstrated in Fig. 6.7. It can be seen from Fig. 6.7(a) and (b) that the HV values of the uncoated specimen before and after compression are quite close and the fluctuations in different sites of the specimen are both small, 31 and 24, respectively. This illustrates a rather homogeneous microstructure for the

uncoated specimen even after compression. Before enumerating the HV values of differently coated specimens after fracture, the electroplating pre-treated specimen was tested to rule out the potential influence of this process on the microhardness of BMGs. The results shown in Fig. 6.7(c) reveal that the plating procedure played a negligible effect on the microhardness evolution. On the other hand, the laterally coated specimen displayed a slightly wider range of hardness values from 498 HV to 539 HV. More interestingly, Fig. 6.7(d) and (e) illustrate that the two end coated and the completely encapsulated specimens both show a sharp deviation of hardness in different sites, ranging 484 HV ~ 554 HV and 462 HV ~ 563 HV, respectively, manifesting that these two BMGs can be considered as networks of soft and hard regions. Thus, it is worthwhile to emphasize that work softening together with work hardening should occur during uniaxial compression of the two end coated and the completely encapsulated samples. In fact, despite that the structural evolution associated with the plastic deformation in BMGs is still not yet clear, it is widely identified that due to shear localization, the atoms in BMGs will rearrange and the coalescence of free volume will engender a decrease of hardness in some local regions such as the shear bands [184]. Macroscopically, the hardness decrease at some regions can be estimated by the function [184]:

$$H=H_m - A\cdot(\frac{1}{d}),\quad d^{-1}=0.14\varepsilon_p, \tag{6.1}$$

where H_m is the original hardness of the BMG; A is a proportionality constant equal to the softening induced by shear bands that are interspaced 1 μm apart; d

is the interspace between shear bands, and is inversely proportional to the plastic strain ε_p. Consistent with the different degrees of hardness drops, the different shear band interspaces d in accordance with the different ε_p values can be seen from Fig. 6.6. Regarding this, the intense drop of hardness for some regions in the most ductile BMG can be clearly understood. On the other hand, if multiple shear bands have been activated during deformation, the intersection of shear bands along different orientations will prohibit the shear propagation and shear localization may cease to prevent shear softening in the mean time, which is akin to the effect of dislocation intersections in crystalline materials [185]. This can enhance the opportunity of "work hardening" in some regions. In addition, on loading, the excess free volume within the entire BMG will be redistributed and the transformed free volume configuration can lead to an inhomogeneous distribution of free volume. It is reasonable to imagine the hardness increase in some areas with the exhausted free volume in the progress of plastic deformation. The work softening and hardening effects during deformation are able to play a positive role in the subsequent plastic strain during compression. The soft regions can act as preferred areas for further initiating shear bands while the hard regions make for impeding the rapid propagation of shear bands. This large heterogeneous microstructure induced ductility has been widely proven previously, as introduced in Chapter 2.

As for the side surface coated BMG, the main contribution of the lateral Cu

coating on the increased density of shear bands lies in the residual compressive stress at the coating/BMG interface brought about by electroplating, and the delaying effect in the shear banding process with the assistance of the lateral confining stress, as has been discussed in the preceding Sections on geometric confinement. Turning to the two end coated samples, as mentioned above, friction is caused by the elastic mismatch between the loading platens and the specimen. The dimensionless Dunders' parameter is a convenient measure to quantitatively assess the elastic mismatch between two contacting materials. This parameter can be calculated based on the following expressions [186]:

$$\beta=\frac{\mu_2(k_1-1)-\mu_1(k_2-1)}{\mu_2(k_1+1)+\mu_1(k_2+1)}; \quad k_i=\frac{3-\nu_i}{1+\nu_i}, \tag{6.2}$$

where μ_1, μ_2 are the shear moduli of the contacting materials 1 and materials 2, respectively. ν_i (the subscript i = 1 and 2) refers to Poisson's ratio of the two contacting materials. According to the above expressions, the degree of the elastic mismatch can be tuned by changing the shear moduli and Poisson's ratios of the contacting materials, and the β parameter decreases with the decrease of the difference between the moduli and Poisson's ratios of the two contacting materials. Given that Poisson's ratio ν = 0.343 and shear modulus μ = 48.3 for Cu coating [187] are between the values for the two contacting materials, ν = 0.295, μ = 78.5 for WC hardened steel [187] and ν = 0.362, μ = 30.1 [4, 188] for the $Zr_{57}Al_{10}Ni_8Cu_{20}Ti_5$ BMG, the β parameter can therefore be reduced by the introduction of solid Cu coatings as a lubricant at the loading boundaries. By substituting these values into equations (6.2), one can get β = 0.126 for the

Zr-based BMG/WC steel platen loading boundaries with the absence of the Cu coating lubricant. With the asistance of a layer of electroplated Cu coating as a lubricant at each end of the BMG specimen, β can be reduced to 0.0631 for the Cu coating/WC steel pair and reduced to 0.0683 for the Zr-based BMG/Cu coating pair, respectively, strongly lessening the effect of frictional boundary restraints. This precipitous decrease of the β parameter can lessen the shear stresses and the resulting "clamping" effect at the loading interfaces, thus reducing the lateral spreading suppression of the material near the ends. Meanwhile, the Cu coating at each end of the BMG is itself compressed, and generates a lateral pressure near the edges of the material [189]. This pressure near the edges of the material can be quantitatively deduced. If the coefficient of friction, μ, at the boundaries is constant, the average pressure to cause deformation can be derived from [142]:

$$\mathrm{P_{av}} = Y[1+\frac{\mu d}{3h}+(\frac{\mu d}{h})^2/12+\cdots], \tag{6.3}$$

in which Y is the true flow stress of the test material, and h/d is the aspect ratio (height-to-diameter ratio). However, if the shear stress at the loading interface remains constant, such as that achieved by the introduction of a Cu coating layer at the interface, the average pressure develops into [142]:

$$\mathrm{P_{av}} = Y+\frac{kd}{3h}, \tag{6.4}$$

in which k refers to the shear strength of the lubricant material. Taking this into consideration, the lateral pressure superimposed by the compressed Cu coatings

is also beneficial for promoting the lateral spreading of the material near the ends. In addition, it is worth to note that the electroplated Cu coatings at the two ends of the BMG may also be beneficial for the plastic deformation of BMGs in two respects. On the one hand, they can help prevent or retard pre-mature crack nucleation from the loading interface corners between the rigid platens and the BMG, where fracture preferentially initiates due to stress concentration at the corners [190-192]. On the other hand, the chances are that the small departures from perpendicularity in alignment between the two ends and the principal axis of the BMG sample cannot be ruled out after the incorporation of electroplated Cu coating at each end. Such departures may also contribute to the enhanced plasticity of the two end coated specimens, as reported by Wu *et al* [193].

As far as the completely encapsulated Zr-based BMG is concerned, with the combination of assistance from the lateral electroplated Cu coating on the side surface and the Cu coating at each end as a solid lubricant, high plasticity is successfully achieved, and the underlying mechanism can be understood in terms of the combined effects of the reduction of frictional boundary restraints as well as geometric confinement.

6.3 Summary

The influence of frictional boundary restraints between the loading platens and the specimen on the compressive deformation behaviour of BGMs was

introduced. By reducing the friction at the loading boundaries, the compressive plasticity of BMGs can be improved. This was confirmed in the two end Cu coated and the completely encapsulated $Zr_{57}Al_{10}Ni_8Cu_{20}Ti_5$ BMGs with substantially higher plasticity than the uncoated specimens. The largest plasticity of 20% achieved in the completely encapsulated $Zr_{57}Al_{10}Ni_8Cu_{20}Ti_5$ BMG is attributable to the combined effects of geometric confinement by the lateral Cu coating as well as the lubricating effect at the loading boundaries between the WC steel platens and the BMG by the solid Cu coating lubricant at each end of the BMG. With the presence of this Cu coating lubricant, the friction reduction at the loading boundaries helped lessen the elastic mismatch between the loading platens and the specimen, and the Cu coatings at the two end was compressed to generate a lateral pressure near the edges of the specimen. Accordingly, the lateral spreading of the material near the ends was promoted and the macroscopic plasticity of the BMG specimen was improved. In addition, an inhomogeneous microstructure was found to form in the two end Cu coated and the completely Cu-coating encapsulated BMGs. The degree of inhomogeneity is closely linked to and directly proportional to the ultimate shear band density and plasticity of the BMGs. The heterogeneous microstructural evolution during loading is believed to be beneficial for toughening the BMGs, with the soft regions acting as preferential sites for initiating multiple shear bands and the hard regions favoring the inhibition of the rapid propagation of shear bands.

Chapter 7 Overall conclusions

A layer of Ni coating was laterally electroplated onto the $Zr_{57}Al_{10}Ni_8Cu_{20}Ti_5$ BMG and the $Fe_{75}Mo_5(P_{50}C_{41.67}B_{8.33})_{20}$ BMG as a form of geometric confinement, and the compression tests of the uncoated and the Ni coated BMGs confirmed that Ni coating electroplating is highly effective in enhancing the compressive plasticity of BMGs. This plasticity enhancement by Ni electroplating is ascribed to the residual compressive stress brought about by the Ni plating process and the geometric confining stress by the Ni coating. These two stresses facilitate the initiation of multiple shear bands and the inhibition of shear banding behavior, thus delaying the unstable final fracture of BMGs. Besides, the effectiveness of the confining effect on the plasticity enhancement of BMGs by Ni coating is found to be closely related to the coating thickness.

By means of electroplating a Cu/Ni bilayered coating onto the side surface of the $Zr_{57}Al_{10}Ni_8Cu_{20}Ti_5$ BMG and comparing the compressive behavior of the Cu/Ni coated $Zr_{57}Al_{10}Ni_8Cu_{20}Ti_5$ BMG with an equivalent thick mono-layered Cu or Ni coated specimen, it was found that the effectiveness of the geometric confinement by a Cu/Ni bilayered coating is superior to that by an equivalent thick pure Cu or pure Ni coating. The thin soft inner Cu layer in the Cu/Ni bilayered coating can behave as a strongly effective "crack buffer zone" to absorb the deformation energy released by BMGs through self-deformation; while the

strong outer Ni layer in the Cu/Ni bilayered coating plays a significant role in imposing a high lateral confining stress during loading. Additionally, the high blocking strength of the strong Cu/Ni interface owing to the modulus mismatch, the slip plane mismatch, and the lattice parameter mismatch between the Cu and Ni layer makes a contribution to the enhanced plasticity.

Interestingly, the largest compressive plasticity of 20% reported in the present work was obtained when completely encapsulating the $Zr_{57}Al_{10}Ni_8Cu_{20}Ti_5$ BMG into Cu coatings by electroplating. This pronounced plasticity, compared with uncoated $Zr_{57}Al_{10}Ni_8Cu_{20}Ti_5$ BMG specimen, is attributable to the combined effects of geometric confinement by the lateral Cu coating as well as the frictional boundary optimization effect at the loading boundaries between the WC steel platens and the BMG. The friction reduction at the loading boundaries achieved by the electroplated Cu coating lubricant helps lessen the elastic mismatch between the loading platens and the specimen. Moreover, the Cu coatings at the two ends can be compressed to generate a radial pressure near the edges of the BMG, thus advancing the lateral spreading of the material near the ends. In addition, the inhomogeneous microstructural evolution is believed to be beneficial for toughening the BMGs, considering that the soft regions can be treated as preferential sites for activating multiple shear bands and the hard regions can act as barriers to hinder the rapid propagation of shear bands.

In short, as a cost-effective and convenient engineering technology, metal electroplating has been demonstrated to be an effective and promising method to toughen BMGs.

Chapter 8 Suggested future work

In addition to the effect of the confining metal coating on the compressive properties of BMGs, it is also of great engineering significance to examine the tensile properties and bending behavior of the BMG/metal coating composite.

Due to the effect of the normal stress, the fracture behavior of BMGs strongly depends on the loading modes. Plasticity in BMGs is visible in compression but essentially almost zero plastic strain is observed in tension. The tensile failure of BMGs originates from the initiation of the round radiating cores on the fractured plane induced by the normal tensile stress and the subsequent catastrophic propagation of these cores towards the outside [194]. Despite the fact that the tensile fracture process is quite distinct from the compressive fracture, tensile deformation is still governed by the activation and dynamic propagation of shear bands, which suggests that constraints through the crystalline coating may be effective in enhancing the tensile ductility of BMGs, although the actual case has yet to be disclosed. Regarding this, related efforts have been previously spent in studying the tensile properties of the crystalline/amorphous alloy laminated structure, and the results revealed that if the strength of the crystalline layer in this laminate approaches or is even higher than that of the metallic glass, the amorphous layer would be constrained by and deform in conformity with the well-bonded crystalline layer, leading to a reasonable macroscopic tensile

elongation [195, 196]. Nevertheless, these works were focused on nano-scale amorphous alloy or micro-scale thick metallic glass ribbons. The tensile behavior of the BMG/crystalline laminate has not been reported to date and is worth investigating in future work.

The compressive strength derived from repeated uniaxial compression tests of a BMG is usually statistically distributed and also the plastic strain is scattered severely for the same BMG specimen [197]. A great variety of subtle imperfections in the sample test geometry such as miscuts or deviations from orthogonality can dramatically influence the compressive results [197]. It is therefore of marked significance to search for another approach to supplement the assessment of plastic deformability (or ductility) of BMGs. Aside from uniaxial compression, bending creates another geometry that can better evaluate the ductility of BMGs. In bend tests, the specimen is subject to both compressive and tensile stresses [198], and shear bands can form in both the tensile and compressive sides of the specimen [199, 200]. Bending deformation of BMGs is inherently stable since the stress that drives shear banding diminishes when the shear bands approach the neutral stress axis [201-203].

During bending deformation, shear bands initiate from the surface at both the compressive and tensile sides of the specimen at a low bending angle. With the increase of bending angle, bending deformation proceeds, and the propagation or

branching of the existing shear bands as well as the formation of new shear bands from the surface are the origin of the increased bending plastic strain [199]. In fact, it is reasonable to expect a higher bending ductility in the coated BMG specimens compared with the uncoated ones. The positive role of the electroplated metal coating on bending ductility is supposed to lie in not only the geometric confinement effect that hinders the rapid propagation of shear bands, but also in the residual compressive stress the electroplating brings about. Enlightened by the widespread exploration of residual compressive stress in improving the mechanical performance of conventional silicate glass components, Greer *et al* [12] reported a shot-peened BMG with improved bending plasticity, which was the combined result of the compressive residual stress, and the pre-existing shear bands in the surface layer of the shot-peened sample. From the standpoint of metal electroplating that can also produce residual compressive stress within the surface layer of a BMG, the bending ductility of a metal coated BMG might be higher than that of an uncoated BMG.

In future work, it is proposed to further use bend tests to characterize the bending ductility of BMGs, and to electroplate a layer of metal coating onto monolithic BMGs to investigate whether the metal coating layer is effective in impeding the shear band propagation and shear sliding along the shear offsets during bending tests. If yes, the strain to failure through the bending tests can be used to quantitatively characterize the bending ductility enhancement by the metal

electroplating.

References:

[1] A. Inoue, Acta Mater. 48 (2000) 279.

[2] W. L. Johnson, MRS Bull. 24 (1999) 42.

[3] A.L. Greer, Science 267 (1995) 1947.

[4] W.H. Wang, C. Dong, C.H. Shek, Mater. Sci. Eng. R 44 (2004) 45.

[5] G.Y. Wang, P.K. Liaw, W.H. Peter, B. Yang, M. Freels, Y. Yokoyama, M.L. Benson, B.A. Green, T.A. Saleh, R.L. McDaniels, R.V. Steward, R.A. Buchanan, C.T. Liu, C.R. Brooks, Intermetallics 12 (2004) 1219.

[6] M. Telford, Mater. Today 7 (2004) 36.

[7] J.H. Tregilgas, Adv. Mater. Proc. 162 (2004) 40.

[8] A.S. Argon, Acta Metall. 27 (1979) 47.

[9] K. Wang, T. Fujita, Y.Q. Zeng, N. Nishiyam, A. Inoue, M.W. Chen, Acta Mater. 56 (2008) 2834.

[10] J.Q. Li, L. Wang, H.W. Cheng, H.F. Zhang, Z.Q. Hub, H.N. Cai, J. Alloys Compd. 478 (2009) 827.

[11] K.M. Flores, R.H. Dauskardt, J. Mech. Phys. Solids 54 (2006) 2418.

[12] Y. Zhang, W.H. Wang, A.L. Greer, Nat. Mater. 5 (2006) 857.

[13] S. Scudino, K.B. Surreddi, G. Wang, J.Eckert, Scripta Mater. 62 (2010) 750.

[14] D.J. Green, R. Tandon, V.M. Sglavo, Science 283 (1999) 1295.

[15] P. Yu, Y.H. Liu, G. Wang, H.Y. Bai, W.H. Wang, J. Mater. Res. 22 (2007) 2384.

[16] H.Q. Li, L. Li, C. Fan, H. Choo, P.K. Liaw, J. Mater. Res. 22 (2007) 508.

[17] Y.C. Choi, S.I. Hong, Scripta Mater. 61 (2009) 481.

[18] X.J. Gu, S.J. Poon, G.J. Shiflet, J. Mater. Res. 22 (2007) 344.

[19] Z.P. Lu, C.T. Liu, J.R. Thompson, W.D. Porter, Phys. Rev. Lett. 92 (2004) 245503.

[20] M. Stoica, J. Eckert, S. Roth, Z.F. Zhang, L. Schultz, W.H. Wang, Intermetallics 13 (2005) 764.

[21] X.M. Huang, C.T. Chang, Z.Y. Chang, X.D. Wang, Q.P. Cao, B.L. Shen, A. Inoue, J.Z. Jiang, J. Alloys Compd. 460 (2008) 708.

[22] K. A. Lee, Y.C. Kim, J.H. Kim, C.S. Lee, J. Namkung, M.C. Kim, Mater. Sci. Eng. A 449-451 (2007) 181.

[23] X.M. Huang, C.T. Chang, Z.Y. Chang, A. Inoue, J.Z. Jiang, Mater. Sci. Eng. A 527 (2010) 1952.

[24] J. X. Zhao, R. T. Qu, F. F. Wu, Z. F. Zhang, B. L. Shen, M. Stoica, J. Eckert, J. Appl. Phys. 105 (2009) 103519.

[25] G. Wang, D. Q. Zhao, H.Y. Bai, M. X. Pan, A. L. Xia, B. S. Han, X. K. Xi, Y. Wu, W. H. Wang, Phys. Rev. Lett. 98 (2007) 235501.

[26] N. Kanani, Electroplating and Electroless Plating of Copper and its Alloys, Finishing Publications Ltd., Stevenage, Herts SG 1 4BL, UK, pp. 78-80, 2003.

[27] W. Chen, G. Ravichandran, J. Am. Ceram. Soc. 79 (1996) 579.

[28] W. Chen, G. Ravichandran, J. Mech. Phys. Solids 45 (1997) 1303.

[29] J.K. Dennis, T.E. Such, Nickel and Chromium Plating, Woodhead Publishing Ltd., Abington Hall, Abington, Cambridge CBI 6AH, England, pp.

72-162, 1993.

[30] W. Clement, R.H. Willens, P. Duwez, Nature 187 (1960) 869.

[31] W.L. Johnson, Bulk metallic glasses-A new engineering material, Curr. Opin. Solid State Mater. Sci.1 (1996) 383.

[32] A.J. Drehman, A.L. Greer, D. Turnbull, Appl. Phys. Lett. 41 (1982) 716.

[33] A. Inoue, T. Zhang, T. Masumuto, Mater. Trans. JIM 30 (1989) 965.

[34] A. Inoue, T. Zhang, T. Masumuto, Mater. Trans. JIM 31 (1990)177.

[35] A. Inoue, T. Nakamura, N. Nishiyama, T. Masumuto, Mater. Trans. JIM 33 (1992) 937.

[36] H.W. Kui, A.L. Greer, D. Turnbull, Appl. Phys. Lett. 45 (1984) 615.

[37] H.W. Kui, D. Turnbull, Appl. Phys. Lett. 47 (1985) 796.

[38] H.S. Chen, Acta Metall. 22 (1974) 1505.

[39] A. Inoue, K. Kita, T. Zhang, T. Masumoto, Mater. Trans. JIM 30 (1989) 722.

[40] A. Inoue, M. Kohinata, A. Tasi, Mater. Trans. JIM, 30 (1989) 378.

[41] A. Peker, W.L. Johnson, J. Appl. Phys. 63 (1993) 2342.

[42] T. Zhang, A. Inoue, T. Masumoto, Mater. Sci. Eng. A 181-182 (1994) 1423.

[43] A. Inoue, Y. Shinohara, J.S. Cook. Mater. Trans. JIM, 36 (1995) 1427.

[44] Y. He, C.E. Price, S.J. Poon, Phil. Mag. Lett. 70 (1994) 371.

[45] Z.F. Zhao, Z. Zhang, P. Wen, M.X. Pan, D.Q. Zhao, W.H. Wang, W.L. Wang, Appl. Phys. Lett. 82 (2003) 4699.

[46] X.H. Lin, W.L. Johnson, J. Appl. Phys. 78 (1995) 6514.

[47] B. Zhang, M.X. Pan, D.Q. Zhao, W.H. Wang, Appl. Phys. Lett. 85 (2004)

61.

[48] H.S. Chen, J.T. Krause, E. Coleman, J. Non-Cryst. Solids 18 (1975) 157.

[49] C. Suryanarayana, A. Inoue. Bulk metallic glasses, Boca Raton, FL : CRC Press, pp. 51-52, 2011.

[50] A. Inoue, Sci. Rep. Res. Inst. Tohoku Univ. A 42 (1996) 1.

[51] A. Inoue, Proc. Jpn. Acad. B 73 (1997) 19.

[52] A. Inoue, Bulk Amorphous Alloys, Trans Tech Publications, Zürich, 1998.

[53] D. Turnbull, J.C. Fisher, J. Chem. Phys. 17 (1949) 71.

[54] T.A. Waniuk, J. Schroers, W.L. Johnson, Appl. Phys. Lett. 78 (2001) 1213.

[55] K. Amiya, A. Inoue, Mater. Trans. JIM 43 (2002) 81.

[56] L. Xia, D. Ding, S.T. Shan, Y.D. Dong, J. Phys. Condens. Matter 18 (2006) 3543.

[57] H, Tan, Y. Zhang, D. Ma, Y.P. Feng, Y. Li, Acta Mater. 51 (2003) 4551.

[58] P. Jia, H. Guo, Y. Li, J. Xu, E. Ma, Scripta Mater. 54 (2006) 2165.

[59] A. Inoue, Mater. Trans. JIM 36 (1995) 866.

[60] Z.L. Long, H.Q. Wei, Y.H. Ding, P. Zhang, G.Q. Xie, A. Inoue, J. Alloys Compd. 475 (2009) 207.

[61] Y. Zhang, Y. Li, H. Tan, G.L. Chen, H.A. Davies, J. Non-Cryst. Solids 352 (2006) 5482.

[62] N. Nishiyama, A. Inoue, Mater. Trans. JIM 43 (2002) 1913.

[63] Z.P. Lu, C.T. Liu, Acta Mater. 50 (2002) 3501.

[64] Z.P. Lu, C.T. Liu, Phys. Rev. Lett. 91 (2003) 115505

[65] Z.P. Lu, C.T. Liu, Y. Wu, H. Tan, G.L. Chen, Intermetallics 16 (2008) 410.

[66] S. Mukherjee, J. Schroers, Z. Zhou, W.L. Johnson, W.-K. Rhim, Acta Mater. 52 (2004) 3689.

[67] D.V. Louzguine-Luzgin, A. Inoue, J. Mater. Res. 22 (2007) 1378.

[68] F. Spaepen, Acta Metall. 25 (1977) 407.

[69] M.D. Demetriou, W.L. Johnson, J. Appl. Phys. 95 (2004) 2857.

[70] H.-J. Jun, K.S. Lee, Y.W. Chang, Intermetallics 17 (2009) 463.

[71] T. Kawamura, T. Shibata, A. Inoue, T. Masumoto, Acta Mater. 46 (1998) 253.

[72] J. Schroers, N. Paton, Adv. Mater. Proc. 164 (2006) 61.

[73] G. Wang, S.S. Fang, X.S. Xiao, Q. Hua, H.Z. Gu, Y.D. Dong, Mater. Sci. Eng. A 373 (2004) 217.

[74] H.J. Leamy, H.S. Chen, T.T. Wang, Met. Trans. 3 (1972) 699.

[75] C.A. Pampillo, Scripta Metall. 6 (1972) 915.

[76] T. Masumoto, R. Maddin, Acta Metall. 19 (1971) 725.

[77] C.A. Schuh, T.C. Hufnagel, U. Ramamurty, Acta Mater. 55 (2007) 4067.

[78] H.A. Bruck, T. Christman, W.L. Johnson, Scripta Metall. 30 (1994) 429.

[79] A.I. Taub, F. Spaepen, Acta Metall. 28 (1980) 1781.

[80] M.H. Cohen, D. Turnbull, J. Chem. Phys. 31 (1959) 1164.

[81] P.S. Steif, F. Spaepen, J.W. Hutchinson, Acta Metall. 30 (1982) 447.

[82] L.Y. Chen, Z.D. Fu, X.P. Hao, Q.K. Jiang, X.D. Wang, Q.P. Cao, H. Franz, Y.G. Liu, H.S. Xie, S.L. Zhang, B.Y. Wang, Y.W. Zeng, J.Z. Jiang, Phys. Rev.

Lett. 100 (2008) 075501.

[83] L.Y. Chen, A.D. Setyawan, H. Kato, A. Inoue, G.Q. Zhang, J. Saida, X.D. Wang, Q.P. Cao, J.Z. Jiang, Scripta Mater. 59 (2008) 75.

[84] C.C. Hays, C.P. Kim, W.L. Johnson, Phys. Rev. Lett. 84 (2000) 2901.

[85] K.F. Yao, F. Ruan, Y.Q. Yang, N. Chen, Appl. Phys. Lett. 88 (2006) 122106.

[86] K.B. Kim, J. Das, X.D. Wang, X. Zhang, J. Eckert, S.Yi, Phil. Mag. Lett. 86 (2006) 479.

[87] J.C. Oh, T. Ohkubo, Y.C. Kim, E. Fleury, K. Hono, Scripta Mater. 53 (2005) 165.

[88] J. Pan, L. Liu, K.C. Chan, Scripta Mater. 60 (2009) 822.

[89] X.H. Du, J.C. Huang, K.C. Hsieh, Y.H. Lai, H.M. Chen, J.S.C. Jang, P.K. Liaw, Appl. Phys. Lett. 91 (2007) 131901.

[90] E.S. Park, D.H. Kim, Acta Mater. 54 (2006) 2597.

[91] J. Das, M.B. Tang, K.B. Kim,R. Theissmann, F. Baier, W.H. Wang, J. Eckert, Phys. Rev. Lett. 94 (2005) 205501.

[92] K.B. Kim, J. Das, S. Venkataraman, S. Yi, J. Eckert, Appl. Phys. Lett. 89 (2006) 071908.

[93] D. Schryvers, G.S. Firstov, J.W. Seo, J.V. Humbeeck, Y.N. Koval, Scripta Mater. 36 (1997) 1119.

[94] J.W. Seo, D. Schryvers, Acta Mater. 46 (1998) 1165.

[95] Y.N. Koval, G.S. Firstov, L. Delaey, J.V. Humbeeck, Scripta Metall. Mater. 31 (1994) 799.

[96] Y.N. Koval, G.S. Firstov, A.V. Kotko, Scripta Metall. Mater. 27 (1992) 1611.

[97] S. Pauly, G. Liu, G. Wang, U. Kühn, N. Mattern, J. Eckert, Acta Mater. 57 (2009) 5445.

[98] S. Pauly, J. Das, J. Bednarcik, N. Mattern, K.B. Kim, D.H. Kim, J. Eckert, Scripta Mater. 60 (2009) 431.

[99] S. Pauly, G. Liu, S. Gorantla, G. Wang, U. Kühn, D.H. Kim, J. Eckert, Acta Mater. 58 (2010) 4883.

[100] S. Pauly, S. Gorantla, G.Wang, U. Kühn, J. Eckert, Nature Mater. 9 (2010) 473.

[101] Y. Wu, H. Wang, H.H. Wu, Z.Y. Zhang, X.D. Hui, G.L. Chen, D. Ma, X.L. Wang, Z.P. Lu, Acta Mater. 59 (2011) 2928.

[102] Y. Wu , Y.H. Xiao, G.L. Chen, C.T. Liu, Z.P. Lu, Adv. Mater. 22 (2010) 2770.

[103] S. Pauly, J. Das, C. Duhamel, J. Eckert, Adv. Eng. Mater. 9 (2007) 487.

[104] J. Das, S. Pauly, C. Duhamel, B.C. Wei, J. Eckert, J. Mater. Res. 22 (2007) 326.

[105]Y.F. Sun, B.C. Wei, Y.R. Wang, W.H. Li, T.L. Cheung, C.H. Shek, Appl. Phys. Lett. 87 (2005) 051905.

[106] J. Das, K. B. Kim, W. Xu, B. C. Wei, Z. F. Zhang, W. H. Wang, S. Yi, J. Eckert, Mater. Trans. JIM 47 (2006) 2606.

[107] G.S. Firstov, J. Van Humbeeck, Y.N. Koval, Scripta Mater. 50 (2004) 243.

[108] J.J. Lewandowski, W.H. Wang, A.L. Greer, Phil. Mag. Lett. 85 (2005) 77.

[109] J. Schroers, W.L. Johnson, Phys. Rev. Lett. 93 (2004) 255506

[110] X.J. Gu, S.J. Poon, G.J. Shiflet, Appl. Phys. Lett. 88 (2006) 211905.

[111] P. Yu, H.Y. Bai, Mater. Sci. Eng. A 485 (2008) 1.

[112] W.L. Johnson, K. Samwer, Phys. Rev. Lett. 95 (2005) 195501.

[113] A. Kelly, W.R. Tyson, A.H. Cottrell, Philos. Mag. 15 (1967) 567.

[114] K. Sieradzki, A. Rinaldi, C. Friesen, P. Peralta, Acta Mater. 54 (2006) 4533.

[115] V.S. Deshpande, A. Needleman, E.V. der Giessen, J. Mech. Phys. Solids 53 (2005) 2661.

[116] H. Guo, P. F. Yan, Y. B. Wang, J. Tan, Z. F. Zhang, M. L. Sui, E. Ma, Nat. Mater. 6 (2007) 735.

[117] C. A. Volkert, A. Donohue, F. Spaepen, J. Appl. Phys. 103 (2008) 083539.

[118] Y. Wu, H.X. Li, Z.Y. Liu, G.L. Chen, Z.P. Lu, Intermetallics 18 (2010) 157.

[119] W. F. Wu, Z. Han, Y. Li, Appl. Phys. Lett. 93 (2008) 061908.

[120] M. F. Ashby, A. L. Greer, Scripta Mater. 54 (2006) 321.

[121] B.E. Schuster, Q. Wei, T.C. Hufnagel, K.T. Ramesh, Acta Mater. 56 (2008) 5091.

[122] J. Lu, G. Ravichandrana, J. Mater. Res. 18 (2003) 2039.

[123] H.Q. Li, K.X. Tao, C. Fan, P. K. Liaw, Appl. Phys. Lett. 89 (2006) 041921.

[124] H.Q. Li, C. Fan, K.X. Tao, H. Choo, P.K. Liaw, Adv. Mater. 18 (2006) 752.

[125] D.M. Owen, A.J. Rosakis, W.L. Johnson. In: A. Inoue, C.T. Liu (Eds.), Mater. Res. Soc. Symp. Proc. 554 (1999) 419.

[126] T.C. Hufnagel, T. Jiao, Y. Li, L.Q. Xing, K.T. Ramesh, J. Mater. Res. 17

(2002) 1441.

[127] Y. Kawamura, T. Shibata, A. Inoue, T. Masumoto, Scripta Mater. 37 (1997) 431.

[128] T. Mukai, T.G. Nieh, Y. Kawamura, A. Inoue, K. Higashi, Scripta Mater. 46 (2002) 43.

[129] C.A. Schuh, T.G. Neih, Acta Mater. 51 (2003) 5187.

[130] C.A. Schuh, A.S. Argon, T.G. Neih, J. Wadsworth, Philos. Mag. A 83 (2003) 2585.

[131] A.L. Greer, A. Castellero, S.V. Madge, I.T. Walker, J.R. Wilde, Mater. Sci. Eng. A 375-377 (2004) 1182.

[132] C.A. Schuh, T.G. Neih, J. Mater. Res. 19 (2004) 46.

[133] W.H. Jiang, M. Atzmon, J. Mater. Res. 3 (2003) 755.

[134] T.G. Nieh, C.A. Schuh, J. Wadsworth, Y. Li, Intermetallics 10 (2002) 1177.

[135] Z. Han, W.F. Wu, Y. Li, Y.J. Wei, H.J. Gao, Acta Mater. 57 (2009) 1367.

[136] J. J. Lewandowski, A. L. Greer, Nat. Mater. 5 (2006) 15.

[137] B. Yang, M. L. Morrison, P. K. Liaw, R. A. Buchanan, G. Wang, C. T. Liu, M. Denda, Appl. Phys. Lett. 86 (2005) 141904.

[138] K. M. Flores, R. H. Dauskardt, J. Mater. Res. 14 (1999) 638.

[139] H.A. Bruck, A.J. Rosakis, W.L. Johnson, J. Mater. Res. 11 (1996) 503.

[140] J. Lu, G. Ravichandran, W.L. Johnson, Acta Mater. 51 (2003) 3249.

[141] W.F. Ma, H.C. Kou, J.S. Li, H. Chang, L. Zhou, J. Alloys Compd. 472 (2009) 214.

[142] W.F. Hosford, Mechanical behavior of materials. Cambridge University Press, New York, pp. 47-53, 2005.

[143] P. Weidinger, W. Blum, U. Hunsche, A. Hampe, Phys. Status Solidi A 156 (1996) 305.

[144] J.R. Hammerle, W.F. McClure, J. Texture Stud. 2 (1971) 31.

[145] B. Bhushan, Modern Tribology Handbook, vol. 1, CRC Press, 2001.

[146] K.F. Yao, C.Q. Zhang, J. Appl. Phys. 90 (2007) 061901.

[147] S.F. Guo, L. Liu, N. Li, Y. Li, Scripta Mater. 62 (2010) 329.

[148] U. Landau, "Plating-New Prospects for an Old Art", Electrochemistry in Industry, New Directions, U. Landau, E. Yeager and D. Kortan (Eds.), Plenum Press, New York, 1982.

[149] J.W. Dini, Electrodeposition, The Materials Science of Coatings and Substrates. Noyes Publications, Park Ridge, New Jersey, USA , pp. 1-5, 1993.

[150] L. Mirkova, G. Maurin, M. Monev, C. Tsvetkova, J. Appl. Electrochem. 33 (2003) 93.

[151] A.S.M.A. Haseeb, J.P. Celis, J.R. Roos, J. Electrochem. Soc. 141 (1994) 230.

[152] L.Q. Xing, P. Ochin, M. Harmelin, F. Faudot, J. Bigot, J.P. Chevalier, Mater. Sci. Eng. A 220 (1996) 155.

[153] S.F. Guo, Ph.D Thesis, Huazhong University of Science and Technology, China, 2011.

[154] L. Zhang, L.L. Shi, J. Xu, J. Non-Cryst. Solids 355 (2009) 1005.

[155] J.C. Dyre, Rev. Mod. Phys. 78 (2006) 953.

[156] W.H. Jiang, F.X. Liu, P.K. Liaw, H. Choo, J. Appl. Phys. 90 (2007) 181903.

[157] G. Wang, K.C. Chan, L. Xia, P. Yu, J. Shen, W.H. Wang, Acta Mater. 57 (2009) 6146.

[158] E.E. Gdoutos, K. Pilakoutas, C.A. Rodopoulos, Failure analysis of industrial composite materials, New York, McGraw-Hill, p. 9, 2000.

[159] Z.F. Zhang, G. He, H. Zhang, J. Eckert, Scripta Mater. 52 (2005) 945.

[160] L.F. Liu, L.H. Dai, Y.L. Bai, B.C. Wei, J. Eckert, Mater. Chem. Phys. 93 (2005) 174.

[161] F. Spaepen, Acta Metall. 23 (1975) 615.

[162] W. J. Wright, R. B. Schwarz, W.D. Nix, Mater. Sci. Eng. A 319-321 (2001) 229.

[163] E. H. Yoffe, Philos. Mag. 42 (1951) 739.

[164] E. Sharon, J. Fineberg, Philos. Mag. B 78 (1998) 243.

[165] Z.F. Zhang, F.F. Wu, W. Gao, J. Tan, Z.G. Wang, M. Stoica, J. Das, J. Eckert, B.L.Shen, A. Inoue, Appl. Phys. Lett. 89 (2006) 251917.

[166] A.J. Cao, Y.Q. Cheng, E. Ma, Acta Mater. 57 (2009) 5146-5155.

[167] H. Choi-Yim, R. Busch, U. KÖster, W.L. Johnson, Acta Mater. 47 (1999) 2455.

[168] J.L. Zhang, H.B Yu, J.X. Lu, H.Y. Bai, C.H. Shek, Appl. Phys. Lett. 95 (2009) 071906.

[169] Y.H. Liu, G. Wang, R..J. Wang, D.Q. Zhao, M.X. Pan, W.H. Wang, Science

315 (2007) 1385.

[170] S.J. Hearne, J.A. Floro. J. Appl. Phys. 97 (2005) 014901.

[171] J. J. Lewandowski, X. J. Gu, A. Shamimi Nouri, S. J. Poon, G. J. Shiflet, Appl. Phys. Lett. 92 (2008) 091918.

[172] X. J. Gu, S.J. Poon, G.J. Shiflet, M. Widom, Acta Mater. 56 (2008) 88.

[173] S. E. Hadian, D. R. Gabe, Surface Coatings Technol. 122 (1999) 118.

[174] M.F. Ashby, S.D. Hallam, Acta Metall. 34 (1986) 497.

[175] H.C. Heard, C.F. Cline, J. Mater. Sci. 15 (1980) 1889.

[176] S.I. Rao, P.M. Hazzledine. Philos. Mag. A 80 (2000) 2011.

[177] D. Cheng, Z.J. Yan, L. Yan, Thin Solid Films 515 (2007) 3698.

[178] J.G.M. van Mier, Fracture Processes of Concrete: Assessment of Materials Parameter for Fracture Models, CRC Press, Boca Raton, FL, 1997.

[179] T.C. Hsu, A.J. Young, J. Strain Anal. 2 (1967) 159.

[180] A.G. Atkins, A.S. Weinstein, International Journal of Mechanical Sciences 12 (1970) 641.

[181] C. Fan, A. Inoue, J. Appl. Phys. 77 (2000) 46.

[182] S.V. Madge, P. Sharma, D.V. Louzguine-Luzgin, A.L. Greer, A. Inoue, Scripta Mater. 62 (2010) 210.

[183] H. Kimura, T. Masumoto, Acta Metall. 31(1983) 231.

[184] S. Xie, E.P. George, Acta Mater. 56 (2008) 5202.

[185] K. F. Yao, F. Ruan, Y. Q. Yang, N. Chen, J. Appl. Phys. 88 (2006) 122106.

[186] S. Schmauder, M. Meyer, Z. Metallkd. 83 (1992) 524.

[187] C.J. Smithells, Materials Referece Books, fifth ed., Butterworth, London, 1976.

[188] J.J. Lewandowski, A.K. Thurston, P. Lowhaphandu, Mater. Res. Soc. Symp. Proc. 754 (2003) 307.

[189] J. Chakrabarty, Theory of Plasticity, third ed., Elsevier Butterworth-Heinemann Oxford, 2006.

[190] A.R. Akisanya, C.S. Meng, J. Mech. Phys. Solids 51 (2003) 27.

[191] A. Kotousov, Int. J. Adhesion Adhesives 27 (2007) 647

[192] Z. Wu, Eng. Fract. Mech. 73 (2006) 953.

[193] W.F. Wu, Y. Li, C.A. Schuh, Philos. Mag. 88 (2008) 71.

[194] Z.F. Zhang, J. Eckert, L. Schultz, Acta Mater. 51 (2003) 1167.

[195] X.F. Li, K.F. Zhang, G.F. Wang. Mater. Lett. 61 (2007) 4901.

[196] T.G. Nieh, T.W. Barbee, J. Wadsworth. Scripta Mater. 41 (1999) 929.

[197] W. F. Wu, Y. Li, C. A. Schuh, Philos. Mag. 88 (2008) 71.

[198] D.C. Hofmann, J.-Y. Suh, A. Wiest, G. Duan, M.-L. Lind, M.D. Demetriou, W.L. Johnson, Nature 451 (2008) 1085.

[199] Y. Hu, J.F. Li, T. Lin, Y.H. Zhou, J. Mater. Res. 24 (2009) 3590.

[200] Y.H. Liu, W.H. Wang, J. Non-Cryst. Solids 354 (2008) 5570.

[201] R.D. Conner,W.L. Johnson, N.E. Paton, W.D. Nix. J. Appl. Phys. 94 (2003) 904.

[202] G. Ravichandran, A. Molinari, Acta Mater. 53 (2005) 4087.

[203] R.D. Conner, Yi Li, W.D. Nix, W.L. Johnson, Acta Mater. 52 (2004) 2429.